Stem Cell Reports
Article
ISSCR
OPEN ACCESS

Accelerated Maturation of Human Stem Cell-Derived Pancreatic Progenitor Cells into Insulin-Secreting Cells in Immunodeficient Rats Relative to Mice

Jennifer E. Bruin,[1] Ali Asadi,[1] Jessica K. Fox,[1] Suheda Erener,[1] Alireza Rezania,[2] and Timothy J. Kieffer[1,3,*]
[1]Laboratory of Molecular and Cellular Medicine, Department of Cellular and Physiological Sciences, Life Sciences Institute, University of British Columbia, 2350 Health Sciences Mall, Vancouver, BC V6T 1Z3, Canada
[2]BetaLogics Venture, Janssen R&D LLC, 1000 Route 202 South, Room J108A, Raritan, NJ 08869, USA
[3]Department of Surgery, University of British Columbia, 950 West 10th Avenue, Vancouver, BC V5Z 1M9, Canada
*Correspondence: tim.kieffer@ubc.ca
http://dx.doi.org/10.1016/j.stemcr.2015.10.013

SUMMARY

Pluripotent human embryonic stem cells (hESCs) are a potential source of transplantable cells for treating patients with diabetes. To investigate the impact of the host recipient on hESC-derived pancreatic progenitor cell maturation, cells were transplanted into immunodeficient SCID-beige mice or nude rats. Following the transplant, basal human C-peptide levels were consistently higher in mice compared with rats, but only rats showed robust meal- and glucose-responsive human C-peptide secretion by 19–21 weeks. Grafts from rats contained a higher proportion of insulin:glucagon immunoreactivity, fewer exocrine cells, and improved expression of mature β cell markers compared with mice. Moreover, ECM-related genes were enriched, the collagen network was denser, and blood vessels were more intricately integrated into the engrafted endocrine tissue in rats relative to mice. Overall, hESC-derived pancreatic progenitor cells matured faster in nude rats compared with SCID-beige mice, indicating that the host recipient can greatly influence the fate of immature pancreatic progenitor cells post-transplantation.

INTRODUCTION

Patients with type 1 diabetes suffer from a severe deficiency in insulin production by pancreatic islets as a result of immune-mediated destruction of pancreatic β cells. Insulin independence can be achieved by transplantation of cadaveric human islets (Shapiro, 2011), but because of the scarcity of donor tissue, the field is exploring the potential use of scalable human embryonic stem cell (hESC)-derived pancreatic cells as an alternative cell source. We have demonstrated previously that hESC-derived pancreatic progenitor cells develop over several months in vivo into insulin-secreting cells capable of reversing hyperglycemia in a mouse model of type 1 diabetes (Rezania et al., 2012, 2013; Bruin et al., 2013). Interestingly, the maturation process was accelerated when mice were exposed to chronic hyperglycemia but unaffected by exposure to long-term insulin therapy, short-term exendin-4 treatment, oral anti-diabetic medications, or high-fat diets (Bruin et al., 2013, 2015). In addition, we recently reported a revised differentiation protocol that generated glucose-responsive insulin-secreting cells in vitro and required a much shorter maturation period (~6 weeks) following transplantation to reverse hyperglycemia in mice (Rezania et al., 2014). Given the uncertainty surrounding the complex host environment and variables that may affect the maturation process in vivo, advancing the differentiation protocols in vitro prior to transplantation may be advantageous. Nevertheless, hESC-derived pancreatic progenitor cells are currently being tested for safety, tolerability, and efficacy in a phase 1/2 clinical trial by Viacyte (ClinicalTrials.gov identifier NCT02239354). Therefore, although newer differentiation protocols have been reported (Pagliuca et al., 2014; Rezania et al., 2014; Russ et al., 2015), it remains important to understand the development of pancreatic progenitor cells in vivo because clinical trials are underway in patients with diabetes.

There are several obvious differences between the preclinical transplant recipients tested to date (immunodeficient mice) and the target patient population, including the species, distinct metabolic profiles, and large size difference. Although rats are not directly comparable with humans, their physiology is reportedly more similar to humans than mice, particularly in terms of cardiovascular parameters (Davies and Morris, 1993). We have demonstrated previously that hESC-derived grafts were capable of robust glucose-stimulated insulin secretion (GSIS) after just 14 weeks in nude rats, whereas GSIS was not observed until after 30 weeks in similar studies with severe combined immunodeficiency (SCID)-beige mice (Rezania et al., 2012). However, these studies were performed at different facilities and with different batches of cells, so we could not make direct comparisons between species. Interestingly, others have reported that hESC-derived pancreatic progenitor cells did not efficiently differentiate into pancreatic endocrine tissue following transplantation in nude rats (Matveyenko et al., 2010). The authors speculated that the nude rat may be a less accommodating host environment compared with immunodeficient mice (Matveyenko et al., 2010). To address these conflicting observations, we

performed a carefully controlled study within a single research facility to directly compare the in vivo development of hESC-derived pancreatic progenitor cells from the same preparation and transplanted in parallel into either immunodeficient nude rats or SCID-beige mice.

RESULTS

hESC-Derived Insulin-Producing Cells Develop Faster and Function Better in Rats Than in Mice

Pluripotent H1 cells were differentiated into pancreatic progenitor cells over 14 days, resulting in a population containing 17% endocrine cells (synaptophysin+). Chromogranin+ endocrine cells, coexpressed NKX2.2 but were largely negative for NKX6.1, a sign of immaturity (Figure S1). The differentiated cells were ~80% PDX1+, ~50% NKX6.1+, ~18% PAX6+, and ~15% Ki67+ (Figure S1). Pluripotent cells (OCT3/4+) were not detected in the differentiated population at the time of transplantation (Figure S1). This preparation of pancreatic progenitor cells was then transplanted under the kidney capsule of either SCID-beige mice (~5 million cells) or nude rats (~7 million cells). To determine whether increasing the number of transplanted cells would affect maturation in vivo, we also compared glucose-stimulated human C-peptide secretion at 28 weeks following transplantation of either 5, 10, or 20 million hESC-derived progenitor cells in a separate study (Figure S2). Although the amount of human C-peptide tended to increase with the higher doses of cells, the degree of glucose-responsiveness (indicated by the C-peptide stimulation index) of hESC-derived cells did not differ between doses (Figure S2).

At the time of transplantation, nude rats weighed ~ ten times more than SCID-beige mice on average (Figure S3A), but rats were transplanted with less than two times the amount of cells (Figure S3B). Therefore, although the kidney grafts in rats were slightly larger than in mice (Figures S3C and S3E), they were not scaled proportionately relative to the profound difference in body weight and, consequently, blood volume of the host (Figure S3D). Interestingly, despite this discrepancy in dosing, plasma human C-peptide concentrations were indistinguishable between species after a meal challenge (Figure 1A). However, rats had significantly lower basal human C-peptide levels compared with mice between 19 and 32 weeks post-transplantation (Figure 1A), which translated into an improved stimulation index for meal-induced human C-peptide secretion (Figure S4). At just 19 weeks, hESC-derived cells from rats secreted significantly more human C-peptide under fed versus fasted conditions, whereas there was no meal response by engrafted cells in mice at any stage (Figure 1A; Figure S4). Blood glucose levels were similar between species after an overnight fast, but mice had consistently higher glucose excursions following a meal compared with rats at all ages examined, regardless of graft maturity (Figure 1B). Mice also experienced significantly higher glucose excursions during an oral glucose challenge relative to rats (Figure 1C). Glucose-stimulated human C-peptide secretion was observed in rats at 21 weeks post-transplantation, whereas human C-peptide levels dropped below baseline levels following the glucose challenge in mice (Figure 1D). There was a trend toward lower basal human C-peptide levels after a 6-hr fast in rats compared with mice, although this did not reach statistical significance ($p = 0.06$; Figure 1E). Under random-fed conditions, human insulin, glucagon, and GLP-1 levels were all significantly lower in rats relative to mice at 22 or 33 weeks post-transplantation (Figure 1F).

Kidney Capsule Grafts from Rats Contain More Mature β Cells Than Those Harvested from Mice

At 22/33 weeks post-transplantation, grafts from rats expressed significantly higher levels of mature β cell genes, including *INS*, *NKX6.1*, *MAFA*, *PAX6*, *ABCC8*, *PCSK1*, and *IAPP*, as well as significantly lower levels of the immature pancreatic endocrine marker *NEUROG3* and mature α cell genes, *GCG* and *ARX*, relative to grafts from mice (Figure 2). Furthermore, grafts from rats contained approximately three times more insulin relative to glucagon immunoreactivity, whereas glucagon immunoreactivity was almost twice as prevalent as insulin in grafts from mice (Figures 3A and 3C). Glucagon-positive cells in both species uniformly co-expressed the α cell transcription factor ARX (Figure S5A). Relative to the total endocrine area, grafts from rats were ~40%–50% insulin-positive, whereas grafts from mice were ~10%–25% insulin-positive (Figures 3A and 3C). There also appeared to be more pancreatic polypeptide (PP)-positive cells in grafts from rats, although cells expressing PP, somatostatin, or ghrelin were much less prominent and, therefore, not quantified (Figure S5B). At the gene level, there were no differences in *SST* or *PPY* expression between species, but grafts from mice had approximately two times more *GHRL* transcript compared with grafts from rats (Figure 2). Overall, hESC-derived progenitor cells developed more efficiently into the endocrine lineage in rats compared with mice, as indicated by the significantly reduced trypsin-positive area (Figures 3B and 3D), higher proportion of synaptophysin:trypsin immunoreactivity (Figures 3B and 3D), and decreased gene expression of the exocrine marker *PTF1A* in grafts from rats versus mice (Figure 2). The presence of non-endodermal germ layers was not detected in kidney capsule grafts from either species (Table S1), unlike grafts generated with our earlier differentiation protocol that, on occasion, contained regions of bone and cartilage tissues (Rezania et al., 2012).

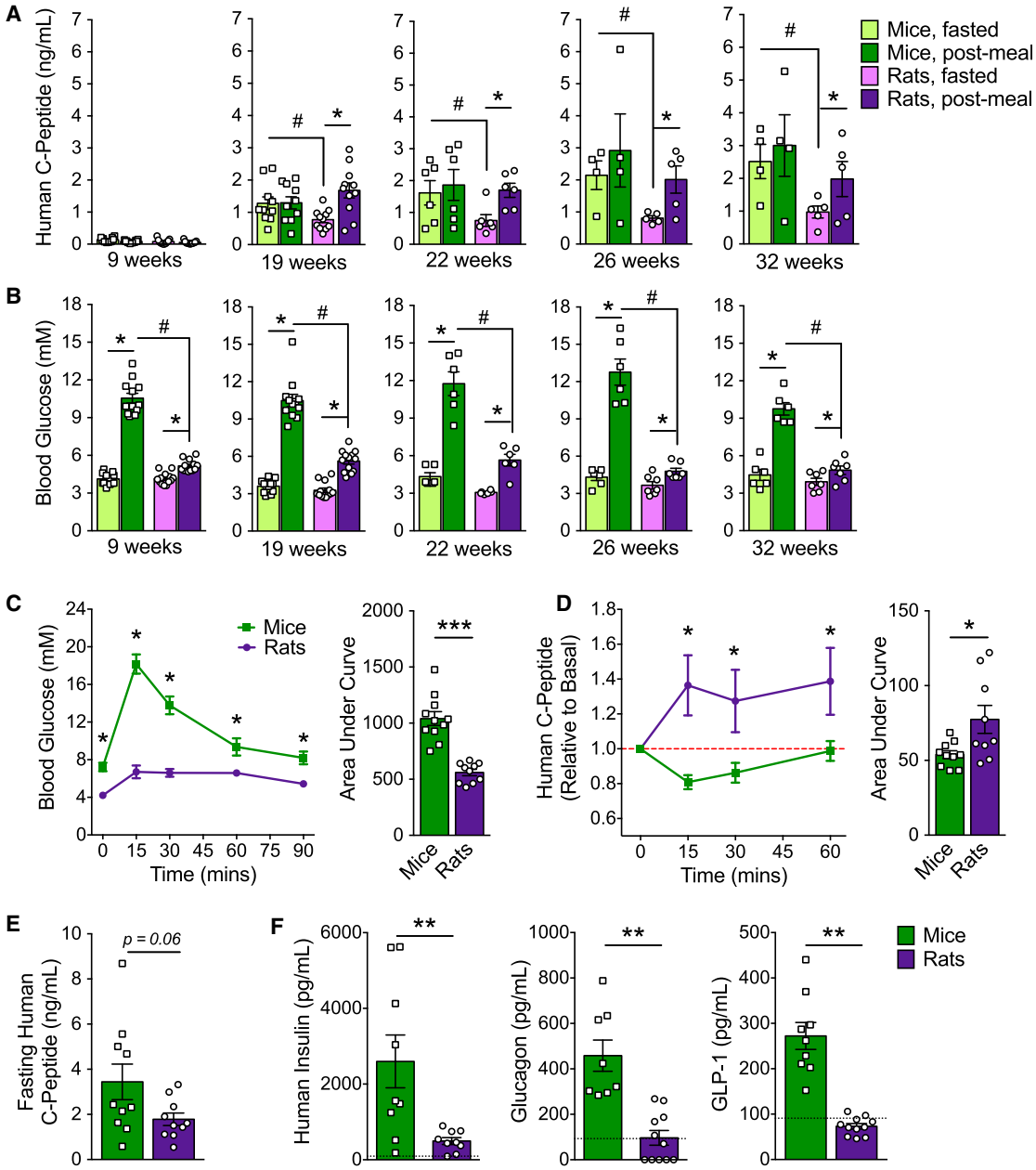

Figure 1. Improved Glycemic Control and Better Graft Function in Rats Compared with Mice

(A and B) Human C-peptide (A) and blood glucose levels (B) after an overnight fast and 45 min following an oral mixed meal between 9–32 weeks post-transplantation (n = 4–11 animals/group). *p < 0.05, paired t test (fast versus fed); #p < 0.05, one-way ANOVA with Student-Neuman-Keuls (SNK) test.

(C–E) Blood glucose (C) and human C-peptide levels (D and E) following a 6-hr morning fast and subsequent oral glucose challenge at 21 weeks post-transplantation (n = 10–11 animals/group). Human C-peptide levels are presented as (D) fold change relative to basal (red dashed line) or (E) raw values at time 0. For line graphs, *p < 0.05, two-way repeated-measures ANOVA with Sidak post hoc test (mouse versus rat). For area under the curve, *p < 0.05, ***p < 0.001; two-tailed t test.

(F) Plasma human insulin, glucagon, and GLP-1 levels at 22 or 33 weeks post-transplantation (n = 10 animals/group). The black dashed line indicates the lower limit of detection for each analyte. **p < 0.01, two-tailed t test.

Data are presented as mean ± SEM plus individual biological replicates in bar graphs. See Figure S4 for the human C-peptide stimulation index following meal challenges.

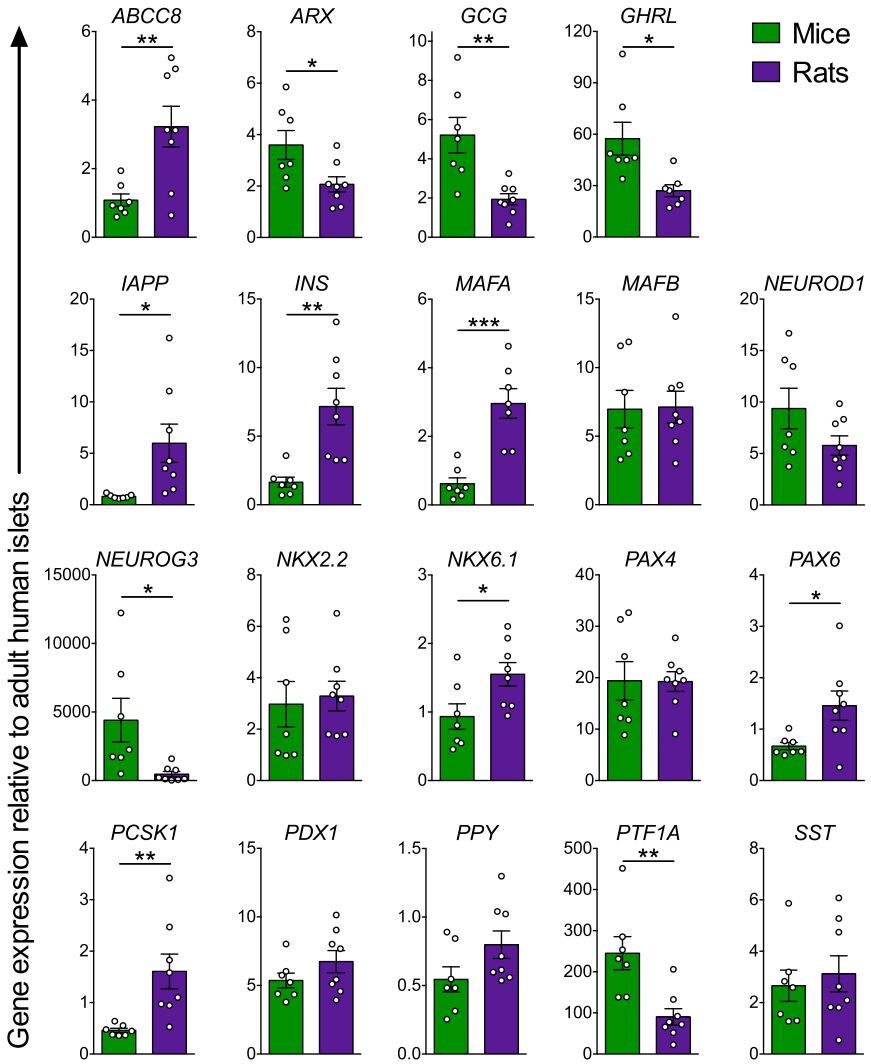

Figure 2. Grafts from Rats Expressed Higher Levels of Mature β Cell Genes and Reduced Pancreatic α and Exocrine Cell Markers Compared with Mice

Relative gene expression (normalized to adult human islets) of pancreas-related genes in hESC-derived engrafted cells harvested at 22 or 33 weeks post-transplantation (n = 7–8 animals/group). *p < 0.05, **p < 0.01, ***p < 0.001, two-tailed t test (mouse versus rat). Data are presented as mean ± SEM plus individual biological replicates.

However, ducts associated with mucin and goblet cells, which are atypical of pancreatic duct morphology, were detected in several grafts from both species (Table S1). The independent pathology analysis is provided in Table S1.

Because the higher levels of mature β cell genes in grafts from rats may simply reflect the higher proportion of β cells, we next examined protein expression for a range of mature β cell markers to assess the maturation status of individual hESC-derived insulin-positive cells. Expression of the β cell transcription factors PDX1, NKX6.1, and NKX2.2 was similar between species (Figure 4A). However, MAFA expression was highly heterogenous in grafts from mice, ranging from weak or absent to strong nuclear immunoreactivity within the insulin-positive cell population (Figure 4B, white arrows). In contrast, MAFA immunoreactivity was consistently robust and nuclear within insulin-positive cells in grafts from rats, which supports the observed ~8-fold increase in *MAFA* gene levels in grafts from rats compared with mice (Figure 2). Thyroid hormone was recently reported to be a physiological stimulus for β cell maturation in neonatal rats and to regulate *Mafa* expression (Aguayo-Mazzucato et al., 2013). Interestingly, we found that endogenous total triiodothyronine (T3, active thyroid hormone) levels were more than twice as high in rats than in mice at 22 weeks post-transplantation (mice, 0.761 ± 0.11 ng/ml; rats, 1.84 ± 0.15 ng/ml; n = 6/species).

SERPINB2 (serpin peptidase inhibitor, clade B [ovalbumin], member 2) and DGCR2 (DiGeorge syndrome critical region gene 2) were recently reported to be unique markers of mature β cells (Lindskog et al., 2012). We observed robust SERPINB2 and DGCR2 immunoreactivity in adult human β cells and grafts from rats compared with heterogenous expression in both immature human fetal β cells and grafts from mice (Figure S6). Another

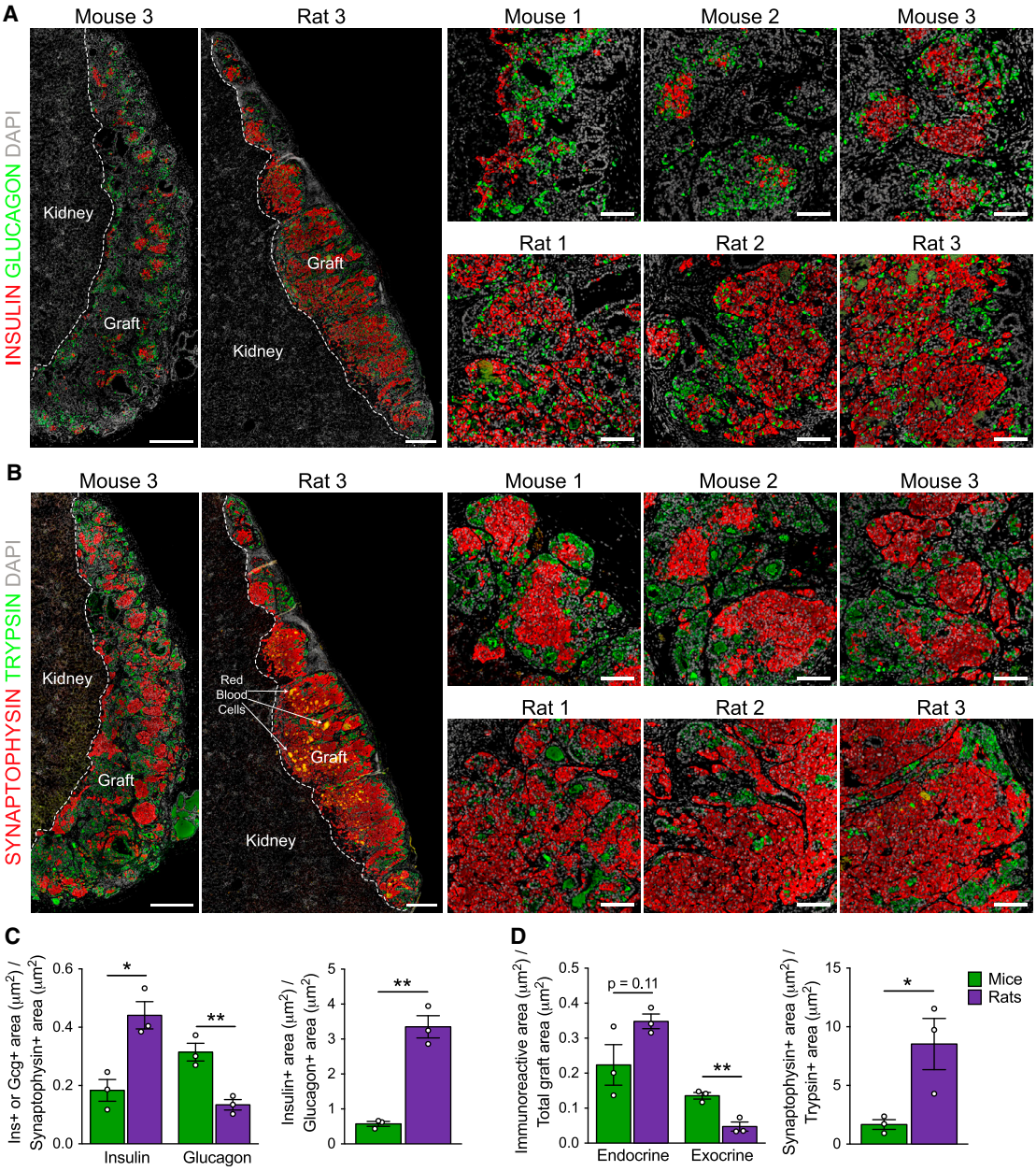

Figure 3. Grafts from Rats Contained a Higher Proportion of Insulin:Glucagon and Synaptophysin:Trypsin Immunoreactivity Compared with Grafts from Mice

(A and B) Representative immunofluorescence images of whole hESC-derived grafts (graft and kidney tissue is delineated by a dashed white line; scale bars, 500 μm) and higher-magnification insets (scale bars, 100 μm) at 22 weeks post-transplantation. Shown are (A) insulin (red) and glucagon (green) and (B) synaptophysin (red, endocrine marker) and trypsin (green, exocrine marker). DAPI nuclear staining is shown in gray in all images.

(C) Area of insulin (ins) or glucagon (gcg) immunoreactivity relative to total synaptophysin immunoreactivity and insulin+ area relative to glucagon+ area for each graft.

(D) Area of synaptophysin or trypsin immunoreactivity relative to the total graft area and synaptophysin+ area relative to trypsin+ area for each graft.

*$p < 0.05$, **$p < 0.01$; two-tailed t test. All data are presented as mean ± SEM plus individual biological replicates (n = 3 animals/group). See Figure S5 for additional immunofluorescent staining of hESC-derived grafts.

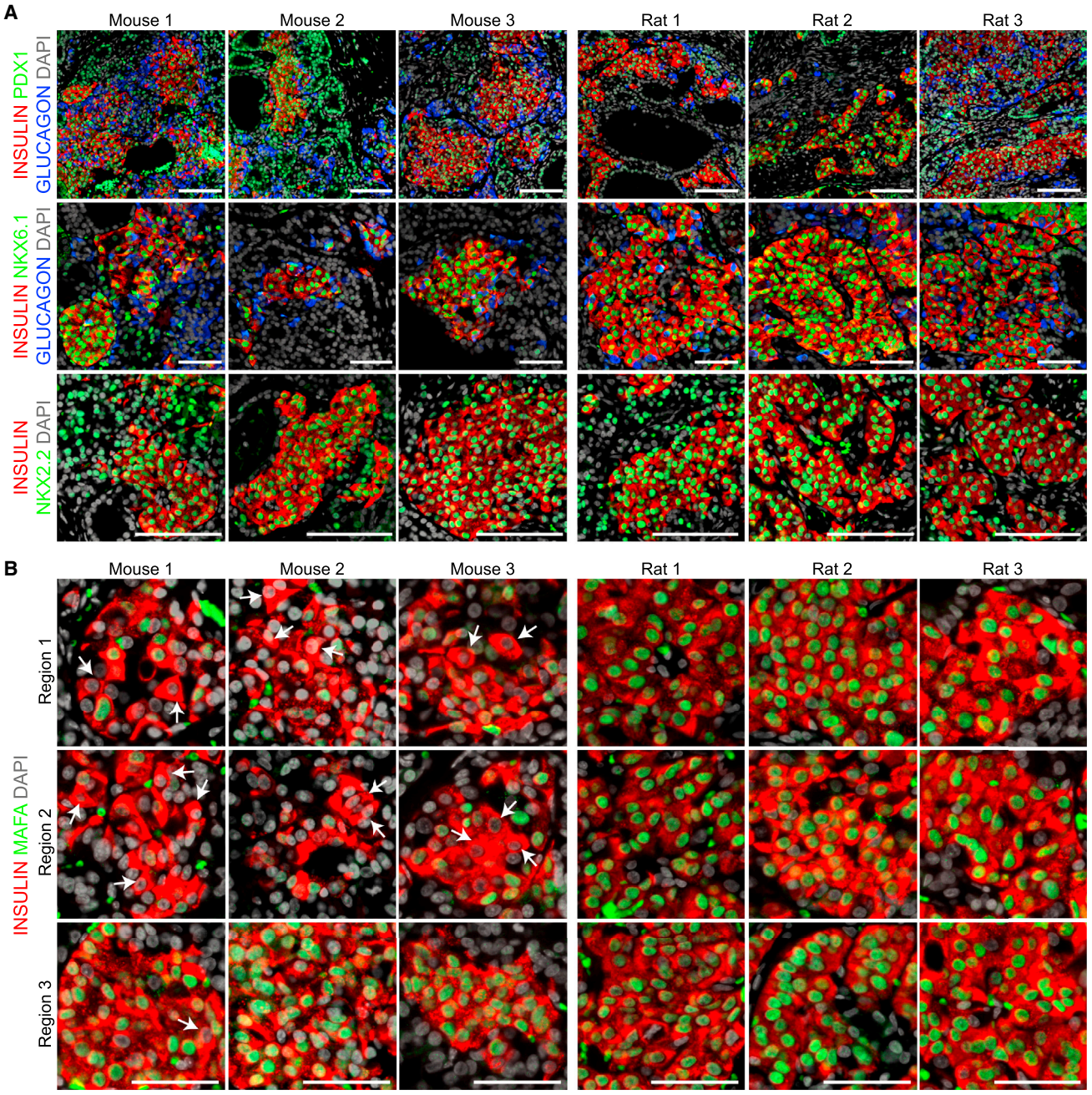

Figure 4. hESC-Derived Insulin-Positive Cells from Both Species Expressed Similar β Cell Transcription Factors Except MAFA Expression Was More Heterogenous in Mice.

(A) Representative immunofluorescent staining of engrafted cells for insulin (red), glucagon (blue), and various transcription factors (green): PDX1, NKX6.1, and NKX2.2 (scale bars, 100 μm).

(B) Three different regions of insulin-positive cells (red) from each graft illustrate the heterogeneity in nuclear MAFA expression (green; white arrows show examples of insulin-positive cells without nuclear MAFA immunoreactivity). Scale bars, 50 μm. DAPI nuclear staining is shown in gray.

See Figure S6 for additional immunofluorescent staining of mature β cell markers in hESC-derived grafts.

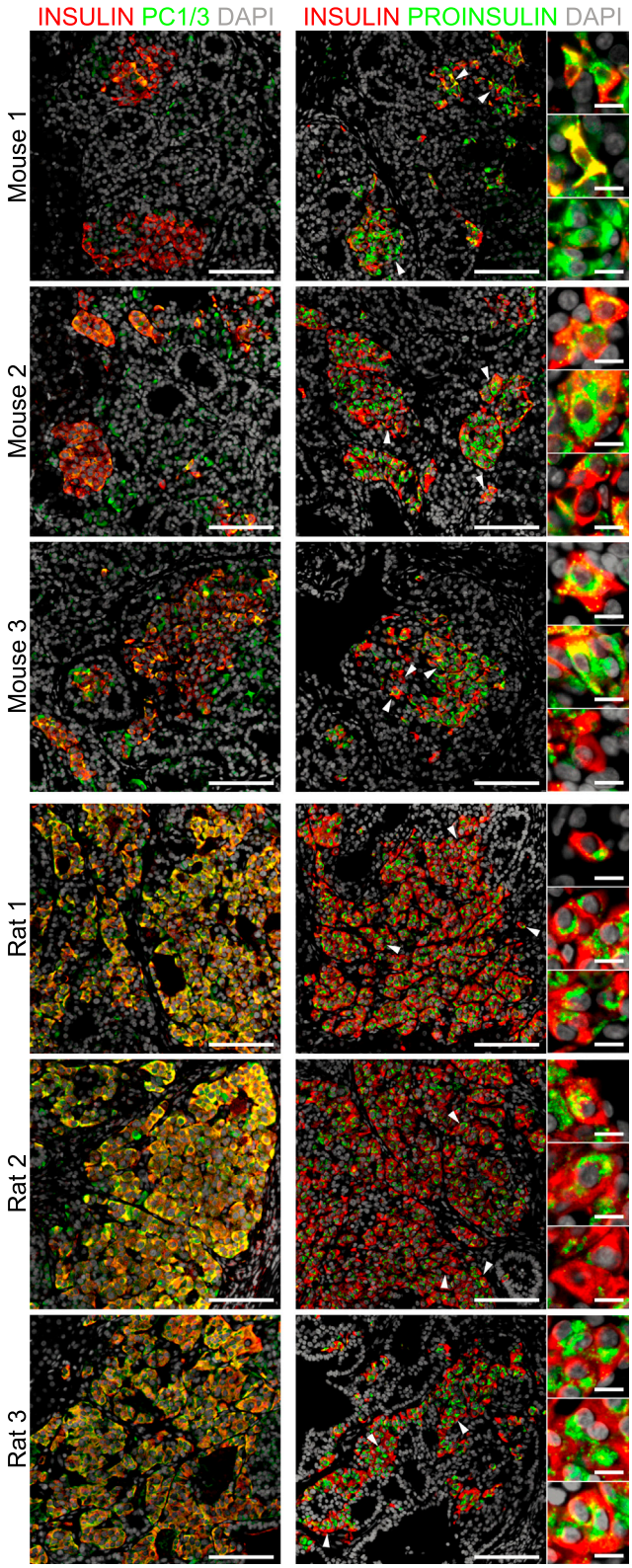

Figure 5. Grafts from Mice Express Less PC1/3 and Inconsistent Proinsulin Immunoreactivity Compared with Rats

Representative immunofluorescent staining of engrafted cells for insulin (red) and either PC1/3 or proinsulin (green). DAPI nuclear staining is shown in gray. White arrowheads indicate cells that are magnified in the insets on the right. Proinsulin immunoreactivity was almost exclusively punctate and perinuclear in grafts from rats, whereas variable patterns of immunoreactivity were observed in mice. Scale bars represent 100 μm (low-magnification images) and 10 μm (high-magnification insets).

feature of mature β cells is the presence of prohormone convertase enzymes, which convert proinsulin into mature insulin and C-peptide (Asadi et al., 2015). *PCSK1* gene expression was significantly higher in grafts from rats compared with mice (Figure 2), and almost all engrafted insulin-positive cells coexpressed PC1/3 in rats (Figure 5). Proinsulin immunoreactivity in grafts from rats was also uniformly punctate and perinuclear (Figure 5), suggesting that non-processed proinsulin is localized within the *trans*-Golgi network, as expected in human β cells (Asadi et al., 2015). In contrast, engrafted insulin-positive cells in mice contained highly heterogenous and generally weaker coexpression of PC1/3, which resulted in diverse patterns of proinsulin immunoreactivity, including cells with intense perinuclear and/or cytoplasmic immunoreactivity (Figure 5). Collectively, graft analysis indicates that hESC-derived progenitor cells developed into a more mature pancreatic endocrine phenotype in rats compared with mice, with a bias toward the development of β cells instead of α cells.

Grafts from Rats Are Better Vascularized and Express Higher Levels of Genes Involved in Extracellular Matrix Organization Than Grafts from Mice

Since vascularization is a critical factor for islet graft survival and function post-transplantation (Pepper et al., 2013), we measured a panel of secreted human proteins related to angiogenesis. Mice had significantly higher circulating levels of human vascular endothelial growth factor C (VEGF-C) and basic fibroblast growth factor (bFGF) than rats, but all other angiogenic proteins were similar between species (Figure 6A). Interestingly, we also observed a clear increase in the density and distribution of red blood cells in grafts from rats compared with mice (Figure 6B; red blood cell area as percent of total graft area; mice, 0.95% ± 0.33%; rats, 4.44% ± 1.40%), suggesting that hESC-derived grafts were better vascularized in rats. Lectins (e.g., wheat germ agglutinin [WGA]) are carbohydrate-binding proteins commonly used for marking vasculature (Jilani et al., 2003; Robertson et al., 2015). Substantial lectin staining was observed in grafts from mice and rats, indicating that both were highly vascularized, but lectin

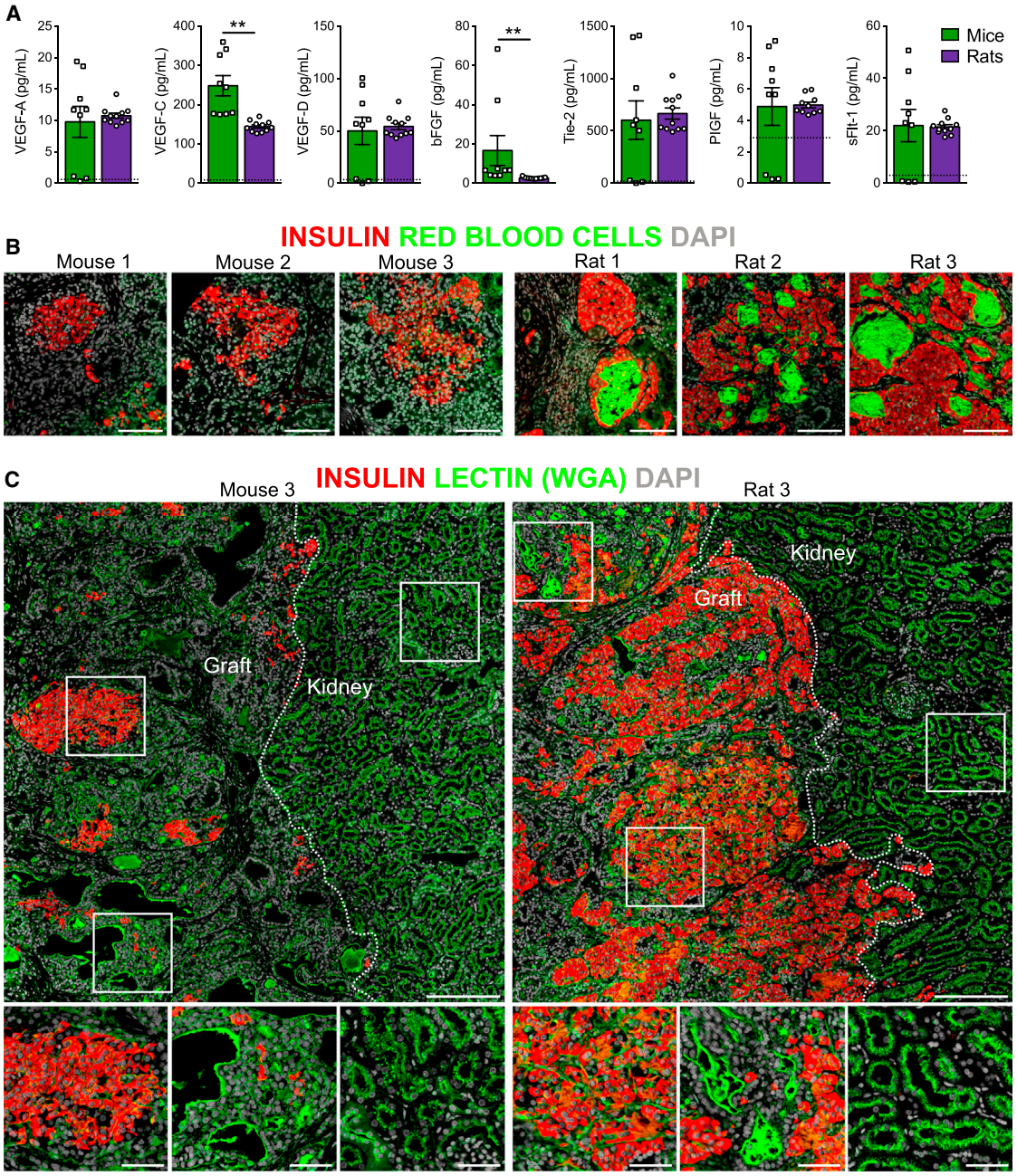

Figure 6. Engrafted hESC-Derived Cells Were More Highly Vascularized in Rats than in Mice

(A) Plasma levels of angiogenesis-related secreted proteins at 22 or 33 weeks post-transplantation (n = 9–11 animals/group). The dashed black line indicates the lower limit of detection on each assay. **p < 0.01, two-tailed t test. Data are presented as mean ± SEM plus individual biological replicates.

(B) Examples of autofluorescent red blood cells (green) among hESC-derived, insulin-positive endocrine tissue (red) in grafts from mice and rats at 22 weeks post-transplantation. Scale bars, 100 μm.

(C) Representative immunofluorescent staining of hESC-derived cells at 22 weeks post-transplantation for insulin (red) and lectin (wheat germ agglutinin, green). DAPI nuclear staining is shown in gray for all images. Kidney and graft tissues are delineated by dashed white lines, and white boxes indicate regions shown at higher magnification below. Scale bars, 200 μm (low-magnification images) and 20 μm (high-magnification insets).

staining was noticeably increased within insulin-positive, islet-like structures in grafts from rats (Figure 6C).

To investigate other pathways that may be involved in promoting β cell maturation in rats, we performed an unbiased gene chip analysis of hESC-derived graft tissue from both species at 22 weeks post-transplantation. Notably, these data revealed robust upregulation of genes related to extracellular matrix (ECM) structure and organization in grafts from rats compared with mice (Figure 7A). For example, five genes from the collagen family (*COL3A1*, *COL1A1*, *COL15A1*, *COL6A3*, and *COL1A2*) were all upregulated more than 13-fold in grafts from rats compared with mice, along with genes such as *LUM* (lumican), *VCAN* (versican), *FBN1* (fibrillin 1), and *DCN* (decorin), which all encode for important structural components of the ECM (Figure 7A). A list of genes that were significantly enriched >5-fold in mouse grafts relative to rat grafts is provided in Table S2. To further investigate the observed changes in ECM-related genes, we next examined circulating levels of human matrix metalloproteinases (MMPs), which are involved in matrix remodeling. Interestingly, at both 22 and 33 weeks post-transplantation, rats had significantly higher plasma levels of human MMP1 and reduced MMP3 levels compared with mice (Figure 7B). MMP9 levels were not different between species (data not shown). Masson's trichrome staining of engrafted cells confirmed that there were clear differences in the ECM between species (Figure 7D). Grafts in rats were supported by a highly dense collagen layer on the outer surface of the kidney capsule as well as a compact collagen network intricately embedded throughout the hESC-derived cells, whereas grafts in mice contained less collagen overall, and the collagen network was much looser and stained lighter (Figure 7D). Masson's trichrome staining of adult human pancreas tissue demonstrated that human islets are normally supported by a complex collagen matrix both on the periphery and also embedded throughout the islet core (Figure 7C).

Metal-binding metallothioneins (*MT1G*, *MT1X*, and *MT2A*) were also robustly upregulated in grafts from rats compared with mice (Figure 7A). In rodent and human β cell lines (INS1 and EndoC-βH1, respectively), we found that *MT1* expression was profoundly upregulated in response to cellular stress, including exposure to interleukin 1β (IL-1β) alone, a cytokine cocktail (tumor necrosis factor α [TNFα], IL-1β, and interferon γ [IFNγ]), or H_2O_2 (Figure S7A). To determine whether engrafted cells from mice and rats produced different cytokine profiles, we measured a panel of human cytokines in the circulation at 22 and 33 weeks post-transplantation. Interestingly, most of the cytokines measured were near or below the limit of detection, including MIP1β, MCP-1, MCP-4, IP-10, thymus- and activation-regulated chemokine (TARC), Eotaxin, Eotaxin-3, and macrophage-derived chemokine (MDC) (Figure S7B). In contrast, human IL-8 levels were well into the linear detection range of the assay for the majority of samples and were significantly higher in mice compared with rats (Figure S7B).

DISCUSSION

Following transplantation into immunodeficient mice, immature hESC-derived pancreatic progenitor cells develop over a lengthy maturation period into glucose-responsive, insulin secreting cells (Rezania et al., 2012; Bruin et al., 2013), although this process remains poorly understood. The aim of this study was to determine whether the host species affects the development of hESC-derived progenitor cells in vivo. Interestingly, cells engrafted into nude rats secreted human C-peptide in response to both meal and glucose challenges at a much earlier time compared with cells transplanted into SCID-beige mice. Furthermore, grafts from rats contained a significantly higher proportion of mature β cells, increased expression of ECM-related genes, a more complex collagen matrix, and improved vascularization compared with grafts from mice. These data confirm our previous observation that hESC-derived, insulin-secreting cells were glucose-responsive after a relatively short (14-week) maturation period in nude rats (Rezania et al., 2012), and our head-to-head comparison of mice versus rats indicates that this accelerated maturation can likely be attributed to environmental factors within the host milieu.

Based largely on evidence from preclinical studies in immunodeficient mice (Kroon et al., 2008; Kelly et al., 2011; Rezania et al., 2012, 2013; Bruin et al., 2013; Motté et al., 2014), the safety of hESC-derived pancreatic progenitor cells is now being evaluated clinically in a small cohort of patients with type 1 diabetes. However, ongoing preclinical studies in rodent models are still necessary to predict how progenitor cells may behave in a widely variable patient population. Although rats are not an ideal model for humans, their physiology is reportedly more similar to humans than mice (Davies and Morris, 1993). Blood glucose levels in healthy humans typically range from 4.4–6.1 mM and can rise to nearly 7.8 mM after a full meal (International Diabetes Federation, 2011). Similarly, nude rats in our study had fasting blood glucose levels of between ~3–5 mM and an average peak of 5.5 or 6.7 mM following a meal or glucose challenge, respectively. Unlike humans and rats, SCID-beige mice had relatively high fasting glucose levels (average of 7.2 mM) and dramatic glucose fluctuations peaking at 10 or 18 mM, on average, following a meal or glucose challenge, respectively.

A

Genes Enriched in hESC-derived Grafts from Nude Rats								
Gene ID	Gene Name	Gene ID	Rats		Mouse		Ratio	p-value
			Mean	SEM	Mean	SEM		
NM_002345	Lumican	LUM	49.33	1.27	1.51	1.55	32.57	0.0046
AI813758	Collagen, type III, alpha 1	COL3A1	251.72	1.38	8.24	3.44	30.55	0.0429
AI743621	Collagen, type I, alpha 1	COL1A1	85.48	1.79	2.83	1.41	30.24	0.0233
NM_001855	Collagen, type XV, alpha 1	COL15A1	36.88	1.99	1.41	1.27	26.24	0.0369
NM_003118	Secreted protein, acidic, cysteine-rich	SPARC	278.73	1.36	11.26	2.79	24.76	0.0335
NM_004369	Collagen, type VI, alpha 3	COL6A3	90.52	1.53	4.52	2.46	20.01	0.0408
BF218922	Versican	VCAN	39.85	1.61	2.12	1.29	18.8	0.0198
NM_000138	Fibrillin 1	FBN1	32.76	1.79	1.83	1.01	17.87	0.0309
AV700059	Osteoglycin	OGN	29.87	1.75	1.96	1.56	15.25	0.0414
NM_004684	SPARC-like 1 (hevin)	SPARCL1	36.92	1.70	2.47	1.61	14.93	0.0394
NM_000089	Collagen, type I, alpha 2	COL1A2	365.51	1.29	27.18	1.46	13.45	0.0092
NM_000900	Matrix Gla protein	MGP	82.58	1.58	6.20	1.75	13.31	0.0371
AF138302	Decorin	DCN	45.99	1.59	3.52	1.49	13.07	0.0310
Z95331	Fibulin 1	-	19.48	1.61	1.99	1.03	9.81	0.0338
NM_005950	Metallothionein 1G	MT1G	122.61	1.41	14.71	1.62	8.34	0.0337
AW089415	Secreted frizzled-related protein 4	SFRP4	24.94	1.44	3.04	1.38	8.22	0.0279
NM_005952	Metallothionein 1X	MT1X	97.14	1.11	16.15	1.14	6.01	0.0017
NM_005953	Metallothionein 2A	MT2A	145.17	1.15	25.69	1.31	5.65	0.0080

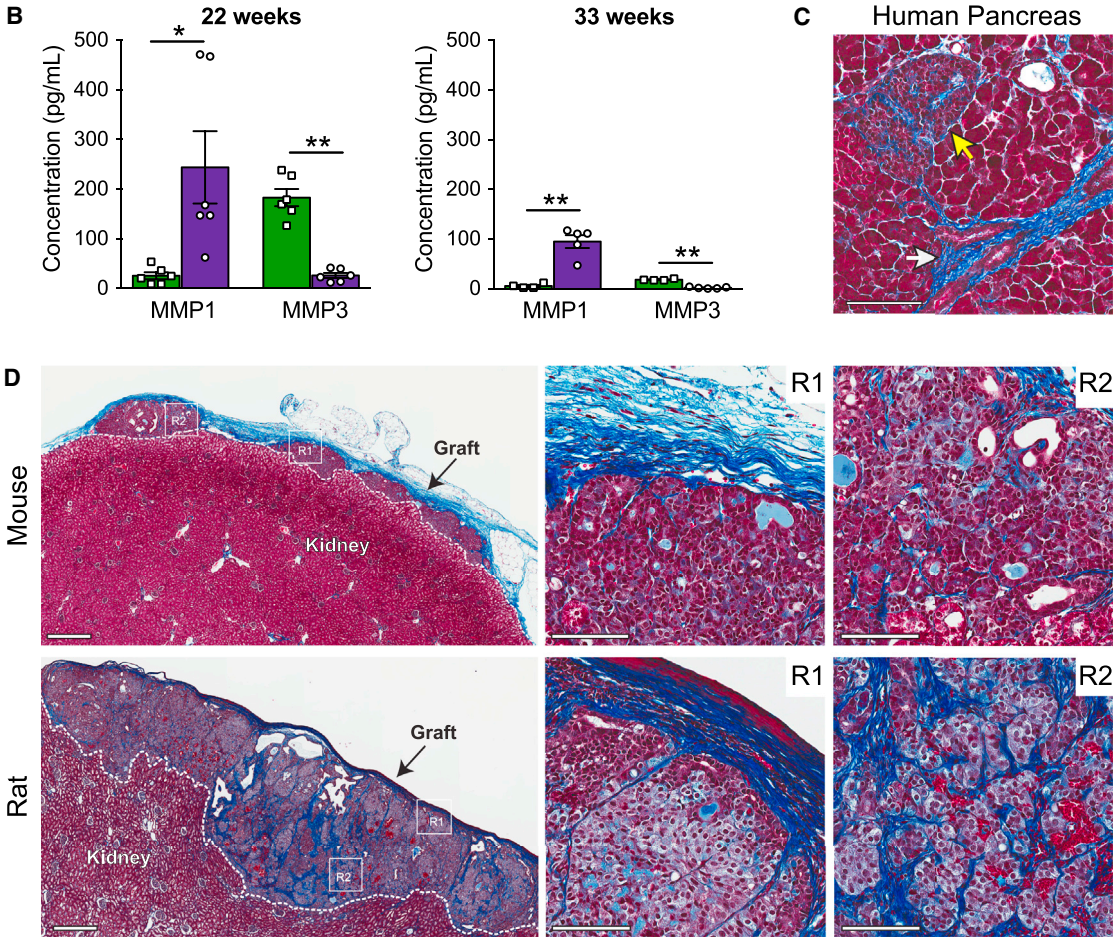

Figure 7. Grafts from Rats Were Enriched for Genes Related to Extracellular Matrix Composition and Remodeling and Were Densely Integrated with Collagen Fibers

(A) List of all genes significantly enriched >5-fold in grafts from rats relative to mice at 22 weeks post-transplantation based on microarray analysis (n = 3 animals/group).

(legend continued on next page)

Another advantage of moving to a larger model is the insight gained into scaling up cell dosing to accommodate a larger transplant recipient. Our studies revealed that the dose of pancreatic progenitor cells does not need to be scaled proportionately with body size to produce therapeutic levels of human insulin. Rats received less than two times the amount of cells despite having approximately ten times the blood volume of mice, and, yet, circulating human C-peptide levels were similar between species. Importantly, the grafts did not simply expand to accommodate the larger host but, rather, matured into better functioning β cells compared with the smaller host. We also confirmed in a separate study, that implanting higher numbers of progenitor cells itself does not affect the glucose responsiveness of hESC-derived insulin-secreting cells post-transplantation. Another consideration for predicting cell dosages in humans is that rodents are relatively insensitive to human insulin (Pepper et al., 2009), meaning that fewer human progenitor cells may be required per unit of body weight to reverse diabetes in patients compared with rodent models. For instance, although diabetic mice typically require 2,000–4,000 human islet equivalents (IEQs) to achieve normoglycemia (~80,000–160,000 IEQs/kg), human patients typically require only ~5,000–10,000 IEQs/kg (Graham et al., 2011). Taken together, these data suggest that the dose of hESC-derived progenitor cells required for humans might be lower than previously predicted based on mouse models.

The fate of hESC-derived pancreatic progenitor cells differed substantially following transplantation in SCID-beige mice versus nude rats. As early as 19 weeks post-transplantation, rats had significantly lower fasting human C-peptide levels and enhanced meal- and glucose-responsive C-peptide secretion compared with mice. One possibility is that the accelerated maturation was driven by differences in immune competence between the two rodent strains. SCID-beige mice possess two autosomal recessive mutations (SCID [*Prkdc*^{scid}] and beige [*Lyst*^{bg}]) that result in lack of B and T lymphocytes as well as defective natural killer (NK) cells (MacDougall et al., 1990), whereas the athymic Rowett nude (RNU) rat is deficient only in T lymphocytes (Cash et al., 1993). Interestingly, when fetal lung xenografts were implanted under the kidney capsule of SCID-beige mice versus nude rats, there were increased inflammation and signs of graft rejection by 4 weeks post-transplantation in nude rats, and the authors speculated that this was likely because of the presence of NK cells in nude rats (De Paepe et al., 2012). In contrast, pancreatic progenitor cells thrived in nude rats for up to 33 weeks in our study despite the presence of NK cells. Others have also shown that hESC-derived progenitor cells matured similarly in different strains of immunodeficient mice, including B6-TCR$\alpha^{-/-}$ (nonfunctional T cells), B6-RAG$^{-/-}$ (nonfunctional T/B cells), non-obese diabetic (NOD)-SCID (nonfunctional T/B cells and impaired NK cells), and NOD-SCID γ (NSG) mice (nonfunctional T/B cells and nonfunctional NK cells) (Szot et al., 2015), suggesting that the immune competency of the different strains may not have been a critical factor in our study. Another possibility is that exposure to high glucose concentrations may have contributed to high basal insulin production by grafts from mice. Human β cells exposed to high glucose become more active under low-glucose conditions (elevated basal biosynthesis and secretion of insulin) and lose the ability to respond to acute variations in glucose concentrations (Ling and Pipeleers, 1996). These data are also supported by our previous observations that mice with chronic hyperglycemia had higher basal human C-peptide production by hESC-derived cells compared with normoglycemic mice (Bruin et al., 2013).

Rat grafts not only contained a higher proportion of insulin-secreting cells but also a more consistently mature β cell phenotype compared with mice, particularly for immunoreactivity of MAFA, a key transcription factor that regulates glucose-stimulated insulin secretion (Matsuoka et al., 2004; Zhang et al., 2005; Wang et al., 2007), and PC1/3, the dominant prohormone convertase responsible for proinsulin processing (Zhu et al., 2002). Indeed, proinsulin immunoreactivity was uniformly restricted to a perinuclear location in grafts from rats as well as human pancreas (Asadi et al., 2015), indicating efficient human proinsulin processing, whereas grafts from mice contained irregular patterns of proinsulin immunoreactivity. Because *Mafa* is involved in regulating *Pcsk1* expression (Wang et al., 2007), these differences

(B) Plasma concentration of human MMP1 and MMP3 at either 22 or 33 weeks post-transplantation (n = 4–6 animals/group). *p < 0.05, **p < 0.01; two-tailed t test. Data are presented as mean ± SEM plus individual biological replicates.

(C) Masson's trichrome staining of adult human pancreas shows blue collagen fibers surrounding a duct (white arrow) and an islet (yellow arrow). Scale bar, 100 μm.

(D) Masson's trichrome staining of hESC-derived grafts at 22 weeks post-transplantation. Low-magnification images of the whole grafts are shown on the left (scale bars, 500 μm). White dashed lines delineate graft and kidney tissue. White boxes highlight the two regions (R1 and R2) shown at higher magnification to the right (scale bars, 100 μm).

See also Figure S7.

may be a reflection of the improved *MAFA* gene expression and nuclear MAFA immunoreactivity in β cells from grafts in rats compared with mice. Thyroid hormone has been recently proposed as a physiological regulator of β cell maturation in neonatal rats via Mafa activation (Aguayo-Mazzucato et al., 2013), and addition of T3 during late stages of hESC differentiation induces *MAFA* expression in vitro (Rezania et al., 2014). Interestingly, the improved graft function and MAFA levels in nude rats were associated with significantly higher circulating thyroid hormone levels. Therefore, future studies should investigate how modulating thyroid hormone levels in vivo may affect the maturation of hESC-derived β cells.

We performed an unbiased gene profile of immature grafts from mice versus mature grafts from rats at 22 weeks post-transplantation to uncover other pathways associated with improved human β cell maturation in vivo. The most striking finding was that grafts from rats were dramatically enriched for genes related to the structural stability of the ECM, including numerous collagens (*COL3A1*, *COL1A1*, *COL15A1*, *COL6A3*, and *COL1A2*), lumican, versican, and others. We also noted a dramatic, ~25-fold increase in *SPARC,* a gene that encodes a matricellular protein involved in mediating the interaction between cells and the ECM via regulation of collagen (Brekken and Sage, 2001), in grafts from rats compared with mice. Interestingly, *SPARC* gene expression has been strongly associated with the degree of glucose-stimulated insulin secretion in isolated human islets, and overexpression of *SPARC* in cultured rat β cells enhanced glucose-stimulated insulin secretion (Harries et al., 2013). There is also substantial evidence that reconstructing the islet cell-ECM relationship following islet isolation improves cell survival and function both in vitro and following islet transplantation in vivo (Nagata et al., 2001; Hammar et al., 2004; Kaido et al., 2004; Navarro-Alvarez et al., 2008; Salvay et al., 2008; Jalili et al., 2011; Yap et al., 2013). For example, islets embedded within a collagen matrix displayed enhanced glucose-stimulated insulin secretion (Nagata et al., 2001; Jalili et al., 2011; Yap et al., 2013). Similarly, hESC-derived cells with glucose-responsive insulin secretion in rats were embedded in a far more dense and elaborate collagen network compared with the non-responsive insulin-secreting cells in mice. Although these data suggest an association between improved human β cell maturation and the composition of the ECM in the host, it still remains to be determined whether the increased ECM network within rats was a causal factor driving the maturation of hESC-derived β cells.

Our gene chip analysis also revealed a robust upregulation of metallothionein (MT) family members that are involved in metal metabolism and detoxification, as well as reactive oxygen species (ROS) scavenging. Overexpression of MT has been shown to protect mice from streptozotocin (STZ)-induced β cell damage and diabetes (Chen et al., 2001) and to improve islet graft survival following transplantation by protecting islets from hypoxia (Li et al., 2004). Therefore, the robust induction of MT1/2 in grafts from rats may have contributed to the improved function of hESC-derived β cells by providing protection from the generally hypoxic transplant environment. Engrafted endocrine cells were more highly vascularized in rats than in mice, which may also contribute to protecting the developing β cells from hypoxia and providing more rapid delivery of nutrients for promoting secretagogue-induced secretory responses. We also demonstrated that *MT1* expression is highly inducible in rodent and human β cell lines by various cell stress pathways, including exposure to ROS or cytokines. Interestingly, ROS stimulation has been shown recently to enhance β cell differentiation in pancreatic explants ex vivo, and reducing ROS production in vivo resulted in decreased β cell differentiation (Hoarau et al., 2014). Grafts from mice produced ~6-fold more IL-8 than rats, a proinflammatory cytokine that is highly secreted from human islets after culture and into the serum of human islet transplant recipients (Citro et al., 2012). Notably, peri-transplantation administration of reparixin (an IL-8 receptor inhibitor) improved islet graft function and survival in both mice and humans (Citro et al., 2012). Therefore, reducing IL-8 secretion by hESC-derived grafts or preventing IL-8 action post-transplantation may be beneficial to progenitor cell development.

Taken together, these studies provide several clues for understanding the accelerated development of hESC-derived, glucose-responsive β cells within rats, including improved integration of the ECM and vasculature with engrafted cells; induction of metallothionein proteins as a protective response to cellular stress; exposure to lower circulating glucose levels in vivo; higher endogenous thyroid hormone levels, which may contribute to induction of MAFA; and reduced IL-8 secretion by grafts. Clearly further work is required to elucidate the exact mechanism(s) underlying the in vivo development of hESC-derived β cells. These studies also highlight the susceptibility of pancreatic progenitor cells to variation within the host environment. Implantation of progenitor cells into closely related but different species revealed substantial differences in the fate choice between pancreatic endocrine versus exocrine lineages as well as α versus β cell lineages. Because the maturation environment may differ amongst human recipients, future studies should continue to investigate the role of host physiology on progenitor cell differentiation and function following transplantation. Efforts to generate bona fide mature human β cells in vitro (Pagliuca et al.,

2014; Rezania et al., 2014; Russ et al., 2015) should also be pursued to minimize the maturation window required in vivo.

EXPERIMENTAL PROCEDURES

In Vitro Differentiation of hESCs

The H1 hESC line was obtained from the WiCell Research Institute. All experiments at the University of British Columbia (UBC) with H1 cells were approved by the Canadian Stem Cell Oversight Committee and UBC Clinical Research Ethics Board. H1 cells were cultured and differentiated according to our previously published 14-day, four-stage protocol (Bruin et al., 2013). Pancreatic progenitor cell quality was assessed by fluorescence-activated cell sorting (FACS) prior to transplantation, as described previously (Rezania et al., 2012). Details about FACS antibodies are provided in Table S3.

Animal Studies

All experiments were approved by the UBC Animal Care Committee. Male 8- to 10-week-old SCID-beige mice (C.B-*Igh*-1b/GbmsTac-*Prkdc*^{scid}-*Lyst*^{bg}N7, Taconic) and male 8- to 10-week-old nude rats (Crl:NIH-*Foxn1*^{rnu}, Charles River Laboratories) were maintained on a 12-h light/dark cycle with ad libitum access to a standard irradiated diet (Teklad diet no.2918, Harlan Laboratories).

Transplantation of hESC-Derived Pancreatic Progenitor Cells

Animals were anesthetized with inhalable isoflurane and received transplants of hESC-derived pancreatic progenitor cells under the left kidney capsule. For the dose-response study (Figure S2), mice received either 5, 10, or 20 million cells (n = 5–6/group). For the mouse versus rat study, 5 million cells were transplanted into SCID-beige mice (n = 12) and 7 million cells into rats (n = 12) on the same day. Pancreatic progenitor cells were generated from the same differentiation experiment (Figure S1) and divided between the transplant recipients. Progenitor cell clusters were drawn up into PE50 tubing (Intramedic polyethylene tubing, BD Biosciences, catalog no. 427411) using a mechanical micromanipulator. The tubing was sealed with Ligaclips (Ethicon Endo-Surgery, catalog no. LT200) and then spun to pack cells into a compact pellet for transplantation (see Figure S3B for the pelleted cell length). All animals received a single subcutaneous (s.c.) injection of enrofloxacin (Baytril) at the time of transplantation (10 mg/kg, Bayer Animal Health).

In Vivo Assessment of Transplanted Cells

All metabolic analyses were performed in conscious, restrained mice and rats. Blood glucose was tested using a handheld glucometer (Lifescan), and all blood samples were collected via the saphenous vein using heparinized microhematocrit tubes. Meal challenges were performed between 4–32 weeks post-transplantation, during which blood was collected after an overnight fast (16 hr) and a subsequent 45-min feeding period with normal chow. An oral glucose tolerance test (OGTT) was performed at 21 weeks post-transplantation. Animals received an oral bolus of glucose (2 g/kg, Vétoquinol) following a 6-hr morning fast. Cardiac blood was collected at 22 weeks (n = 6/species) and 33 weeks (n = 4–5/species) and stored at −30°C until use. For the dose-response study, blood was collected after an overnight fast and 60 min following an intraperitoneal (i.p.) glucose injection (2 g/kg) at 28 weeks post-transplantation.

Cell Culture

The INS-1 rat insulinoma cell line and EndoC-βH1 human β cell line (provided by Drs. R Scharfmann, and P. Ravassard) were cultured as described in the Supplemental Experimental Procedures. INS-1 and EndoC-βH1 cells were exposed to the following treatments in their respective culture media: 10 ng/ml IL1β alone, cytokine cocktail (10 ng/ml TNF-α [R&D Systems], 10 ng/ml IL1β [Sigma-Aldrich], and 10 ng/ml IFNγ [R&D Systems]), 200 μM H_2O_2 (Sigma Aldrich), and 0.5 mM palmitate (sodium salt, Sigma Aldrich). Palmitate was solubilized in 90% ethanol, heated to 60°C, and used in a 1:100 dilution in culture medium supplemented with fatty acid-free 0.5% BSA (Roche Diagnostics).

Multiplex Assay and ELISA

Human C-peptide was measured by ELISA in plasma collected during oral meal or glucose challenges (catalog no. 80-CPTHU-E01.1, Alpco Diagnostics). Secreted proteins from the engrafted cells were measured in cardiac plasma with multiplex assays (Mesoscale Discovery), including human angiogenesis markers (catalog no. K15190D-1), human chemokines (catalog no. K15001C-1), human matrix metalloproteinases (catalog no. K15034C-1), human insulin, glucagon, and GLP-1 (catalog no. K15160C-1). Total triiodothyronine levels were measured in cardiac plasma by ELISA (Total T3, catalog no. 1700; Alpha Diagnostic International). All assays were performed according to the manufacturer's instructions.

Histology and Immunofluorescent Staining

Engrafted kidneys were harvested at 22 weeks post-transplantation (n = 3/species) and processed for paraffin sectioning as described previously (Asadi et al., 2015). H&E and Masson's trichrome staining were performed using standard protocols and scanned using a ScanScope CS system (Aperio). H&E-stained kidney grafts were analyzed by an independent pathologist for the presence of non-pancreatic tissue and teratoma formation (Wax-it Histology Services; Table S1). Immunofluorescent staining and imaging were performed as described previously (Asadi et al., 2015). Antibody information is provided in Table S4. Vasculature was visualized by staining with lectin (WGA, catalog no. W11261, Life Technologies), which binds to sialic acid and *N*-acetylglucosaminyl residues. Quantification of graft immunoreactivity is described in the Supplemental Experimental Procedures. Human fetal pancreas (gestational week 13) was collected according to protocols approved by the Health Sciences Research Ethics Board at the University of Western Ontario. Adult human pancreas tissue was provided by the Irving K. Barber Human Islet Isolation Laboratory with consent to use it for research purposes.

RNA Analysis

At 22 weeks (n = 3/species) or 33 weeks (n = 4–5/species) post-transplantation, graft tissue was trimmed from the kidney of a subset of animals and stored in RNA*later* (Life Technologies) at −30°C. RNA

was isolated, and gene expression was assessed by real-time PCR with custom Taqman arrays (Applied Biosystems) as described previously (Rezania et al., 2012). Details about RNA isolation from INS1 and EndoC-βH1 cells and subsequent qPCR analysis are described in the Supplemental Experimental Procedures. Human islets from a 58-year-old, non-diabetic female were used as a positive control. Data were normalized to an internal housekeeping gene (*GAPDH*) using the ΔΔCt method. Information regarding primers is provided in Table S5.

Genome-wide analysis was performed on grafts at 22 weeks post-transplantation using the Affymetrix HG U133+ PM array strip (Affymetrix, catalog no. PN 901569). Details about gene chip analysis are provided in the Supplemental Experimental Procedures.

Statistical Analysis

All statistics were performed using GraphPad Prism software. Specific statistical tests for each experiment are described in the figure legends. For all analyses, $p < 0.05$ was considered statistically significant. For area under curve analysis, $y = 0$ was considered the baseline. All data are presented as mean ± SEM with individual biological replicates shown as separate data points.

SUPPLEMENTAL INFORMATION

Supplemental Information includes Supplemental Experimental Procedures, seven figures, and five tables and can be found with this article online at http://dx.doi.org/10.1016/j.stemcr.2015.10.013.

AUTHOR CONTRIBUTIONS

J.E.B. wrote the manuscript. J.E.B., A.R., and T.J.K. contributed to the conception and design of the experiments. J.E.B., A.A., J.K.F., S.E., and A.R. were responsible for the acquisition, analysis, and interpretation of data. All authors contributed to manuscript revisions and approved the final version of the manuscript.

ACKNOWLEDGMENTS

This work was funded by the Canadian Institutes of Health Research (CIHR) Regenerative Medicine and Nanomedicine Initiative, Stem Cell Network (SCN), JDRF, and Stem Cell Technologies. J.E.B. and S.E. were both funded by JDRF postdoctoral fellowships. J.E.B. was also generously funded by a CDA postdoctoral fellowship, the CIHR Transplantation Training Program, and a L'Oréal Canada for Women in Science Research Excellence Fellowship. We thank Dr. Rennian Wang for generously providing the human fetal pancreas tissue and Drs. Garth Warnock and Ziliang Ao for the adult human pancreas tissue. We also thank Ms. Diana S. Rosman-Balzer for assistance with gene chip analysis. A.R. is an employee and shareholder of Janssen R&D, LLC. T.J.K. received financial support from Janssen R&D, LLC for the research described in this article.

Received: June 9, 2015
Revised: October 22, 2015
Accepted: October 23, 2015
Published: November 19, 2015

REFERENCES

Aguayo-Mazzucato, C., Zavacki, A.M., Marinelarena, A., Hollister-Lock, J., El Khattabi, I., Marsili, A., Weir, G.C., Sharma, A., Larsen, P.R., and Bonner-Weir, S. (2013). Thyroid hormone promotes postnatal rat pancreatic β-cell development and glucose-responsive insulin secretion through MAFA. Diabetes *62*, 1569–1580.

Asadi, A., Bruin, J.E., and Kieffer, T.J. (2015). Characterization of antibodies to products of proinsulin processing using immunofluorescence staining of pancreas in multiple species. J. Histochem. Cytochem. *63*, 646–662.

Brekken, R.A., and Sage, E.H. (2001). SPARC, a matricellular protein: at the crossroads of cell-matrix communication. Matrix Biol. *19*, 816–827.

Bruin, J.E., Rezania, A., Xu, J., Narayan, K., Fox, J.K., O'Neil, J.J., and Kieffer, T.J. (2013). Maturation and function of human embryonic stem cell-derived pancreatic progenitors in macroencapsulation devices following transplant into mice. Diabetologia *56*, 1987–1998.

Bruin, J.E., Saber, N., Braun, N., Fox, J.K., Mojibian, M., Asadi, A., Drohan, C., O'Dwyer, S., Rosman-Balzer, D.S., Swiss, V.A., et al. (2015). Treating diet-induced diabetes and obesity with human embryonic stem cell-derived pancreatic progenitor cells and antidiabetic drugs. Stem Cell Reports *4*, 605–620.

Cash, J.M., Remmers, E.F., Goldmuntz, E.A., Crofford, L.J., Zha, H., Hansen, C.T., and Wilder, R.L. (1993). Genetic mapping of the athymic nude (RNU) locus in the rat to a region on chromosome 10. Mamm. Genome *4*, 37–42.

Chen, H., Carlson, E.C., Pellet, L., Moritz, J.T., and Epstein, P.N. (2001). Overexpression of metallothionein in pancreatic beta-cells reduces streptozotocin-induced DNA damage and diabetes. Diabetes *50*, 2040–2046.

Citro, A., Cantarelli, E., Maffi, P., Nano, R., Melzi, R., Mercalli, A., Dugnani, E., Sordi, V., Magistretti, P., Daffonchio, L., et al. (2012). CXCR1/2 inhibition enhances pancreatic islet survival after transplantation. J. Clin. Invest. *122*, 3647–3651.

Davies, B., and Morris, T. (1993). Physiological parameters in laboratory animals and humans. Pharm. Res. *10*, 1093–1095.

De Paepe, M.E., Chu, S., Hall, S., Heger, N.E., Thanos, C., and Mao, Q. (2012). The human fetal lung xenograft: validation as model of microvascular remodeling in the postglandular lung. Pediatr. Pulmonol. *47*, 1192–1203.

Graham, M.L., Bellin, M.D., Papas, K.K., Hering, B.J., and Schuurman, H.J. (2011). Species incompatibilities in the pig-to-macaque islet xenotransplant model affect transplant outcome: a comparison with allotransplantation. Xenotransplantation *18*, 328–342.

Hammar, E., Parnaud, G., Bosco, D., Perriraz, N., Maedler, K., Donath, M., Rouiller, D.G., and Halban, P.A. (2004). Extracellular matrix protects pancreatic beta-cells against apoptosis: role of short- and long-term signaling pathways. Diabetes *53*, 2034–2041.

Harries, L.W., McCulloch, L.J., Holley, J.E., Rawling, T.J., Welters, H.J., and Kos, K. (2013). A role for SPARC in the moderation of human insulin secretion. PLoS ONE *8*, e68253.

Hoarau, E., Chandra, V., Rustin, P., Scharfmann, R., and Duvillie, B. (2014). Pro-oxidant/antioxidant balance controls pancreatic β-cell

differentiation through the ERK1/2 pathway. Cell Death Dis. *5*, e1487.

International Diabetes Federation (2011). Guideline for management of postmeal glucose in diabetes. https://www.idf.org/sites/default/files/postmeal%20glucose%20guidelines.pdf.

Jalili, R.B., Moeen Rezakhanlou, A., Hosseini-Tabatabaei, A., Ao, Z., Warnock, G.L., and Ghahary, A. (2011). Fibroblast populated collagen matrix promotes islet survival and reduces the number of islets required for diabetes reversal. J. Cell. Physiol. *226*, 1813–1819.

Jilani, S.M., Murphy, T.J., Thai, S.N., Eichmann, A., Alva, J.A., and Iruela-Arispe, M.L. (2003). Selective binding of lectins to embryonic chicken vasculature. J. Histochem. Cytochem. *51*, 597–604.

Kaido, T., Yebra, M., Cirulli, V., and Montgomery, A.M. (2004). Regulation of human beta-cell adhesion, motility, and insulin secretion by collagen IV and its receptor alpha1beta1. J. Biol. Chem. *279*, 53762–53769.

Kelly, O.G., Chan, M.Y., Martinson, L.A., Kadoya, K., Ostertag, T.M., Ross, K.G., Richardson, M., Carpenter, M.K., D'Amour, K.A., Kroon, E., et al. (2011). Cell-surface markers for the isolation of pancreatic cell types derived from human embryonic stem cells. Nat. Biotechnol. *29*, 750–756.

Kroon, E., Martinson, L.A., Kadoya, K., Bang, A.G., Kelly, O.G., Eliazer, S., Young, H., Richardson, M., Smart, N.G., Cunningham, J., et al. (2008). Pancreatic endoderm derived from human embryonic stem cells generates glucose-responsive insulin-secreting cells in vivo. Nat. Biotechnol. *26*, 443–452.

Li, X., Chen, H., and Epstein, P.N. (2004). Metallothionein protects islets from hypoxia and extends islet graft survival by scavenging most kinds of reactive oxygen species. J. Biol. Chem. *279*, 765–771.

Lindskog, C., Korsgren, O., Pontén, F., Eriksson, J.W., Johansson, L., and Danielsson, A. (2012). Novel pancreatic beta cell-specific proteins: antibody-based proteomics for identification of new biomarker candidates. J. Proteomics *75*, 2611–2620.

Ling, Z., and Pipeleers, D.G. (1996). Prolonged exposure of human beta cells to elevated glucose levels results in sustained cellular activation leading to a loss of glucose regulation. J. Clin. Invest. *98*, 2805–2812.

MacDougall, J.R., Croy, B.A., Chapeau, C., and Clark, D.A. (1990). Demonstration of a splenic cytotoxic effector cell in mice of genotype SCID/SCID.BG/BG. Cell. Immunol. *130*, 106–117.

Matsuoka, T.A., Artner, I., Henderson, E., Means, A., Sander, M., and Stein, R. (2004). The MafA transcription factor appears to be responsible for tissue-specific expression of insulin. Proc. Natl. Acad. Sci. USA *101*, 2930–2933.

Matveyenko, A.V., Georgia, S., Bhushan, A., and Butler, P.C. (2010). Inconsistent formation and nonfunction of insulin-positive cells from pancreatic endoderm derived from human embryonic stem cells in athymic nude rats. Am. J. Physiol. Endocrinol. Metab. *299*, E713–E720.

Motté, E., Szepessy, E., Suenens, K., Stangé, G., Bomans, M., Jacobs-Tulleneers-Thevissen, D., Ling, Z., Kroon, E., and Pipeleers, D.; Beta Cell Therapy Consortium EU-FP7 (2014). Composition and function of macroencapsulated human embryonic stem cell-derived implants: comparison with clinical human islet cell grafts. Am. J. Physiol. Endocrinol. Metab. *307*, E838–E846.

Nagata, N., Gu, Y., Hori, H., Balamurugan, A.N., Touma, M., Kawakami, Y., Wang, W., Baba, T.T., Satake, A., Nozawa, M., et al. (2001). Evaluation of insulin secretion of isolated rat islets cultured in extracellular matrix. Cell Transplant. *10*, 447–451.

Navarro-Alvarez, N., Rivas-Carrillo, J.D., Soto-Gutierrez, A., Yuasa, T., Okitsu, T., Noguchi, H., Matsumoto, S., Takei, J., Tanaka, N., and Kobayashi, N. (2008). Reestablishment of microenvironment is necessary to maintain in vitro and in vivo human islet function. Cell Transplant. *17*, 111–119.

Pagliuca, F.W., Millman, J.R., Gürtler, M., Segel, M., Van Dervort, A., Ryu, J.H., Peterson, Q.P., Greiner, D., and Melton, D.A. (2014). Generation of functional human pancreatic β cells in vitro. Cell *159*, 428–439.

Pepper, A.R., Gall, C., Mazzuca, D.M., Melling, C.W., and White, D.J. (2009). Diabetic rats and mice are resistant to porcine and human insulin: flawed experimental models for testing islet xenografts. Xenotransplantation *16*, 502–510.

Pepper, A.R., Gala-Lopez, B., Ziff, O., and Shapiro, A.M. (2013). Revascularization of transplanted pancreatic islets and role of the transplantation site. Clin. Dev. Immunol. *2013*, 352315.

Rezania, A., Bruin, J.E., Riedel, M.J., Mojibian, M., Asadi, A., Xu, J., Gauvin, R., Narayan, K., Karanu, F., O'Neil, J.J., et al. (2012). Maturation of human embryonic stem cell-derived pancreatic progenitors into functional islets capable of treating pre-existing diabetes in mice. Diabetes *61*, 2016–2029.

Rezania, A., Bruin, J.E., Xu, J., Narayan, K., Fox, J.K., O'Neil, J.J., and Kieffer, T.J. (2013). Enrichment of human embryonic stem cell-derived NKX6.1-expressing pancreatic progenitor cells accelerates the maturation of insulin-secreting cells in vivo. Stem Cells *31*, 2432–2442.

Rezania, A., Bruin, J.E., Arora, P., Rubin, A., Batushansky, I., Asadi, A., O'Dwyer, S., Quiskamp, N., Mojibian, M., Albrecht, T., et al. (2014). Reversal of diabetes with insulin-producing cells derived in vitro from human pluripotent stem cells. Nat. Biotechnol. *32*, 1121–1133.

Robertson, R.T., Levine, S.T., Haynes, S.M., Gutierrez, P., Baratta, J.L., Tan, Z., and Longmuir, K.J. (2015). Use of labeled tomato lectin for imaging vasculature structures. Histochem. Cell Biol. *143*, 225–234.

Russ, H.A., Parent, A.V., Ringler, J.J., Hennings, T.G., Nair, G.G., Shveygert, M., Guo, T., Puri, S., Haataja, L., Cirulli, V., et al. (2015). Controlled induction of human pancreatic progenitors produces functional beta-like cells in vitro. EMBO J. *34*, 1759–1772.

Salvay, D.M., Rives, C.B., Zhang, X., Chen, F., Kaufman, D.B., Lowe, W.L., Jr., and Shea, L.D. (2008). Extracellular matrix protein-coated scaffolds promote the reversal of diabetes after extrahepatic islet transplantation. Transplantation *85*, 1456–1464.

Shapiro, A.M. (2011). State of the art of clinical islet transplantation and novel protocols of immunosuppression. Curr. Diab. Rep. *11*, 345–354.

Szot, G.L., Yadav, M., Lang, J., Kroon, E., Kerr, J., Kadoya, K., Brandon, E.P., Baetge, E.E., Bour-Jordan, H., and Bluestone, J.A. (2015).

Tolerance induction and reversal of diabetes in mice transplanted with human embryonic stem cell-derived pancreatic endoderm. Cell Stem Cell *16*, 148–157.

Wang, H., Brun, T., Kataoka, K., Sharma, A.J., and Wollheim, C.B. (2007). MAFA controls genes implicated in insulin biosynthesis and secretion. Diabetologia *50*, 348–358.

Yap, W.T., Salvay, D.M., Silliman, M.A., Zhang, X., Bannon, Z.G., Kaufman, D.B., Lowe, W.L., Jr., and Shea, L.D. (2013). Collagen IV-modified scaffolds improve islet survival and function and reduce time to euglycemia. Tissue Eng. Part A *19*, 2361–2372.

Zhang, C., Moriguchi, T., Kajihara, M., Esaki, R., Harada, A., Shimohata, H., Oishi, H., Hamada, M., Morito, N., Hasegawa, K., et al. (2005). MafA is a key regulator of glucose-stimulated insulin secretion. Mol. Cell. Biol. *25*, 4969–4976.

Zhu, X., Orci, L., Carroll, R., Norrbom, C., Ravazzola, M., and Steiner, D.F. (2002). Severe block in processing of proinsulin to insulin accompanied by elevation of des-64,65 proinsulin intermediates in islets of mice lacking prohormone convertase 1/3. Proc. Natl. Acad. Sci. USA *99*, 10299–10304.

Stem Cell Reports, Volume *5*

Supplemental Information

Accelerated Maturation of Human Stem Cell-Derived Pancreatic Progenitor Cells into Insulin-Secreting Cells in Immunodeficient Rats Relative to Mice

Jennifer E. Bruin, Ali Asadi, Jessica K. Fox, Suheda Erener, Alireza Rezania, and Timothy J. Kieffer

Cell Culture

The INS-1 rat insulinoma cell line was cultured in RPMI-1640 (Life Technologies) containing 11.2 mM glucose and 2 mM L-glutamine. The medium was supplemented with 10% fetal bovine serum (Life Technologies), 1 mM sodium pyruvate (Life Technologies), 10 mM HEPES, and 50 μM 2-mercaptoethanol (Sigma-Aldrich). EndoC-βH1 cells were cultured in wells coated with ECM (1%, Cat # E1270, Sigma Aldrich) and fibronectin (2 μg ml^{-1}, Sigma-Aldrich) and maintained in DMEM (Sigma-Aldrich) that contained 5.6 mM glucose, 2% BSA fraction V (Roche Diagnostics), 50 μM 2-mercaptoethanol, 10 mM nicotinamide (Sigma-Aldrich), 5.5 μg ml^{-1} transferrin (Sigma-Aldrich), 6.7 ng ml^{-1} selenite (Sigma-Aldrich), 100 U/ml penicillin, and 100 μg ml^{-1} streptomycin. Passages were performed when confluence was observed. Both cell lines were cultured at 5% CO_2/95% air at 37°C.

Quantification of Immunofluorescence Staining

Area of immunoreactive cells was quantified within kidney capsule grafts harvested at 22 weeks post-transplant from mice or rats (n = 3 per group). Immunofluorescent staining was performed on three sections per animal, separated by at least 100 μm, and the average value of all three sections was used to represent each graft. Sections were co-immunostained for synaptophysin (endocrine marker) and trypsin (exocrine marker), as well as insulin and glucagon, and whole slide fluorescence scanning was performed as described above. Individual images were stitched together and the entire graft region was quantified using MetaXpress software. Synaptophysin or trypsin immunoreactive positive area was expressed as a percentage of the whole graft area, but since the immunoreactive area does not include the nuclear area the values substantially underrepresent the proportion of the graft that is endocrine or exocrine. The relative proportion of endocrine to exocrine cells was expressed as the area of synaptophysin immunoreactivity relative to trypsin immunoreactivity. The proportion of endocrine area that was either insulin-positive or glucagon-positive was calculated as the total area of insulin or glucagon

immunoreactivity relative to the total area of synaptophysin immunoreactivity. Finally, the proportion of insulin-positive area to glucagon-positive area was also calculated for each graft.

Quantitative RT-PCR

Total RNA from INS1 and EndoC-βH1 cells was isolating using miRCURY Cell and Plant RNA isolation kit (Exiqon, Woburn, CA) following manufacturer`s instructions with the inclusion of a DNAse digestion step. RNA was reverse transcribed using iScript Reverse Transcription Supermix (BioRad, Mississauga, ON). qRT-PCR was performed using the StepOne Real-Time PCR (Applied Biosystems) with SsoFast EvaGreen Supermixes (BioRad, Mississauga, ON).

Gene Chip

RNA from grafts at 22 weeks post-transplant was quantified using a NanoDrop8000 (Thermo Scientific) and RNA samples were reverse transcribed, biotin labeled, purified, and fragmented using the Gene Atlas 3' IVT Express Kit (Affymetrix, Santa Clara, CA; PN 901228), according to the kit protocol. Briefly, 100 ng RNA was combined with the provided Poly-A RNA controls, and was reverse transcribed into "aRNA" using the First-Strand Buffer and Enzyme mix followed by an incubation with the Second-Strand Buffer and Enzyme mix. The aRNA was labeled with Biotin, using the provided IVT Biotin labelling reagents, and incubated at 40°C for 16 hours. The Biotin-labelled aRNA was purified using magnetic beads according to the kit's directions, and the concentration and quality verified using the NanoDrop8000. Ten μg of purified aRNA was fragmented using the Fragmentation buffer and 7.5 μg of aRNA was combined with hybridization controls and a control oligonucleotide provided in the GeneAtlas Hybridization, Wash, and Stain Kit for 3' IVT Arrays (Affymetrix; PN 301531), according to the kit's protocol. This cocktail was hybridized to the Affymetrix HG U133+ PM Array Strip (Affymetrix PN 901569), using the GeneAtlas Hybridization Station, set to 45°C, for 16 hours. The array strip was then washed and stained as directed by the kit, using the GeneAtlas Fluidics Station (Affymetrix). The array was

then placed in the imaging tray and immediately placed in the GeneAtlas Imaging Station. The Hybridization, Fluidics, and Imaging Stations were all operated using the GeneAtlas Instrument Control Software (Version 1.0; Build 1.01.267). The CEL files were imported into Expression Console (Build 1.0.1.20). The intensity files were normalized using the RMA (Robust Multichip Average) method, transformed into Log_2 values, and exported along with the annotations for gene ontology groups.

Table S1: Pathology analysis of engrafted hESC-derived cells at 22 or 33 weeks post-transplant in mice and rats (related to graft characterization in Figures 3-7).

Animal ID	Time Post-Tx	Endoderm Lineages	Ectoderm or Mesoderm Lineages	Other Observations			
				Ducts Without Goblet Cells / Mucin	Ducts With Goblet Cells / Mucin	Fibroblastic Reaction	Inflammation
Mouse 1	22 wks	Pancreatic: Endocrine < Exocrine	NO	YES	YES, FOCAL	NO	Focal Neutrophilic Inflammation
Mouse 2	22 wks	Pancreatic: Endocrine < Exocrine	NO	YES	NO	NO	NO
Mouse 3	22 wks	Pancreatic: Endocrine < Exocrine	NO	YES	YES, FOCAL	YES	NO
Mouse 4	33 wks	Pancreatic: Endocrine > Exocrine	NO	YES	YES, FOCAL	NO	NO
Mouse 5	33 wks	Pancreatic: Mostly Exocrine	NO	YES (MINOR)	NO	NO	Lymphocytic Inflammation
Rat 1	22 wks	Pancreatic: Endocrine > Exocrine	NO	YES	YES	NO	Focal Lymphocytic Inflammation
Rat 2	22 wks	Pancreatic: Endocrine > Exocrine	NO	YES	YES	YES	Lymphocytic Inflammation
Rat 3	22 wks	Pancreatic: Endocrine > Exocrine	NO	YES	NO	NO	Focal Lymphocytic Inflammation
Rat 4	33 wks	Pancreatic: Mostly Endocrine	NO	YES	NO	YES, MARKED	Lymphocytic and Neutrophilic Inflammation
Rat 5	33 wks	Pancreatic: Mostly Endocrine	NO	YES	YES	NO	Focal Lymphocytic Inflammation
Rat 6	33 wks	Pancreatic: Mostly Endocrine	NO	YES	YES	NO	Focal Lymphocytic Inflammation

Table S2: Genes enriched > 5-fold in mouse grafts relative to rat grafts, as determined by gene chip analysis, related to Figure 7A.

Gene ID	Gene Name	Symbol	Rats		Mice		Ratio	P-value
			Mean	SEM	Mean	SEM		
AF020589	Cytochrome c oxidase subunit VIa polypeptide 1	*COX6A1*	2.42	1.12	198.05	2.76	81.87	0.0107
BC029332	Sterol carrier protein 2	-	5.38	1.17	219.94	2.50	40.89	0.0137
AA115963	Hemoglobin, epsilon 1	*HBE1*	12.65	1.19	310.37	2.38	24.54	0.0184
NM_016528	Hydroxyacid oxidase 3 (medium-chain) (HAO3), mRNA.	-	1.87	1.08	33.45	3.15	17.86	0.0441
M14087	HL14 gene encoding beta-galactoside-binding lectin, 3 end, clone 2	-	2.87	1.10	40.79	1.62	14.2	0.0059
AJ243936	Ring finger protein 5	*RNF5*	1.79	1.06	17.74	2.45	9.91	0.0420
NM_017521	FEV (ETS oncogene family)	*FEV*	3.46	1.31	20.96	1.07	6.07	0.0144
AW242315	Prostaglandin E receptor 3 (subtype EP3)	*PTGER3*	2.95	1.23	17.27	1.37	5.86	0.0154
NM_005345	Heat shock 70kDa protein 1A	*HSPA1A*	25.21	1.08	133.59	1.03	5.3	0.0005
AW594320	Ovostatin 2	*OVOS2*	3.15	1.33	16.63	1.24	5.28	0.0262
AL034417	ERBB receptor feedback inhibitor 1	-	9.43	1.31	47.63	1.63	5.05	0.0489

Table S3: Antibody information for FACS, related to Figure S1.

ANTIGEN	CONJUGATED FLUOROPHORE	SPECIES	SOURCE (Catalogue #)	DILUTION
Chromogranin A	None	Rabbit	Dako (# IS502)	1:10
Ki67	Alexa Fluor 647	Mouse	BD (# 561126)	1:20
NKX2.2	None	Mouse	Developmental Studies Hybridoma Bank University of Iowa	1:100
NKX6.1	None	Mouse	Developmental Studies Hybridoma Bank University of Iowa	1:50
PAX6	PE	Mouse	BD (# 561552)	1:20
PDX1	PE	Mouse	BD (# 562161)	1:20
OCT3/4	AF647	Mouse	BD (# 560329)	1:20
Synaptophysin	None	Rabbit	Abcam (# ab52636)	1:40
IgG1, k, Isotype Control	PE	Mouse	BD (# 555749)	1:40
IgG1, k, Isotype control	Alexa Fluor 647	Mouse	BD (# 557732)	1:40
Purified IgG, k Isotype	None	Rabbit	BD (# 550875)	1:1000
Purified IgG, k Isotype	None	Mouse	BD (# 557273)	1:50

Table S4: Antibody information for immunofluorescent staining, related to Figures 3-6 and S5-S7.

ANTIGEN	SPECIES	SOURCE	DILUTION
CK19	Mouse	Dako, Denmark, M 0888	1:100
Glucagon	Mouse	Sigma-Aldrich, G 2654	1:1000
Glucagon(D16G10)	Rabbit	Cell Signaling Technology, 8233P	1:500
Insulin	Guinea Pig	Sigma-Aldrich, I8510	1:1000
Insulin(C27C9)	Rabbit	Cell Signaling Technology, 3014	1:200
Insulin	Mouse	Millipore, 05-1108	1:200
MAFA	Rabbit	Custom Ab, Lifespan Biosciences	1:1000
NKX6.1	Rabbit	Custom Ab, Lifespan Biosciences	1:1000
NKX2.2	Mouse	Developmental Studies Hybridoma Bank; University of Iowa, 74.5A5	1:100
PDX1	Guinea Pig	Abcam, ab47308	1:1000
Somatostatin	Mouse	Beta Cell Biology Consortium, AB1985	1:500
Synaptophysin	Rabbit	Novus Biologicals, NB120-16659	1:50
Trypsin	Sheep	R&D Systems, AF3586	1:100
Proinsulin (GS9A8)	Mouse	Beta Cell Biology Consortium, GS9A8	1:250
PC1/3	Rabbit	Gift from Dr. Lakshmi Devi	1:500
Ghrelin	Rabbit	BioVision, 5991-100	1:200
Pancreatic polypeptide	Goat	R&D Systems, AF6297	1:200
SerpinB2	Rabbit	Novus Biologicals, NBP1-83163	1:100
DGCR2	Rabbit	Novus Biologicals, NBP1-84255	1:25
ARX	Rabbit	Gift from Dr. Collombat	1:500

Table S5: List of qPCR primers, related to Figure 2 and S7.

qPCR SYSTEM	GENE NAME (species)	PRIMER REFERENCE / SEQUENCE
Applied Biosystems PCR array	*GAPDH*	Hs99999905_m1
	ABCC8	Hs00165861_m1
	ARX	Hs00292465_m1
	GCG	Hs00174967_m1
	GHRL	Hs00175082_m1
	IAPP	Hs00169095_m1
	INS	Hs00355773_m1
	MAFA	Hs01651425_s1
	MAFB	Hs00534343_s1
	NEUROD1	Hs00159598_m1
	NEUROG3	Hs00360700_g1
	NKX2.2	Hs00159616_m1
	NKX6.1	Hs00232355_m1
	PAX4	Hs00173014_m1
	PAX6	Hs00240871_m1
	PCSK1	Hs00175619_m1
	PDX1	Hs00236830_m1
	PPY1	Hs00237001_m1
	PTF1A	Hs00603586_g1
	SST	Hs00356144_m1
StepOne Real-Time PCR	*MT1F*-F (human)	CCACTGCTTCTTCGCTTCTCTCTT
	MT1F-R (human)	TCTTCTTGCAGGAGGTGCATTTG
	MT1X-F (human)	CGCTGCGTGTTTTCCTCTTGAT
	MT1X-R (human)	TCTTCTTGCAGGAGGTGCATTTG (common to both *MT1F* and *MT1X*)
	Mt1-F (rat)	CTGAAGTGACGAACAGTGCTG
	Mt1-R (rat)	CAGGCTTTTATTATTCACATGCTCG
	GAPDH-F (human)	TGCACCACCAACTGCTTAGC
	GAPDH-R (human)	GGCATGGACTGTGGTCATGAG
	Gapdh-F (rat)	GATGGTGAAGGTCGGTGTGA
	Gapdh-R (rat)	CTCCTGGAAGATGGTGATGGG

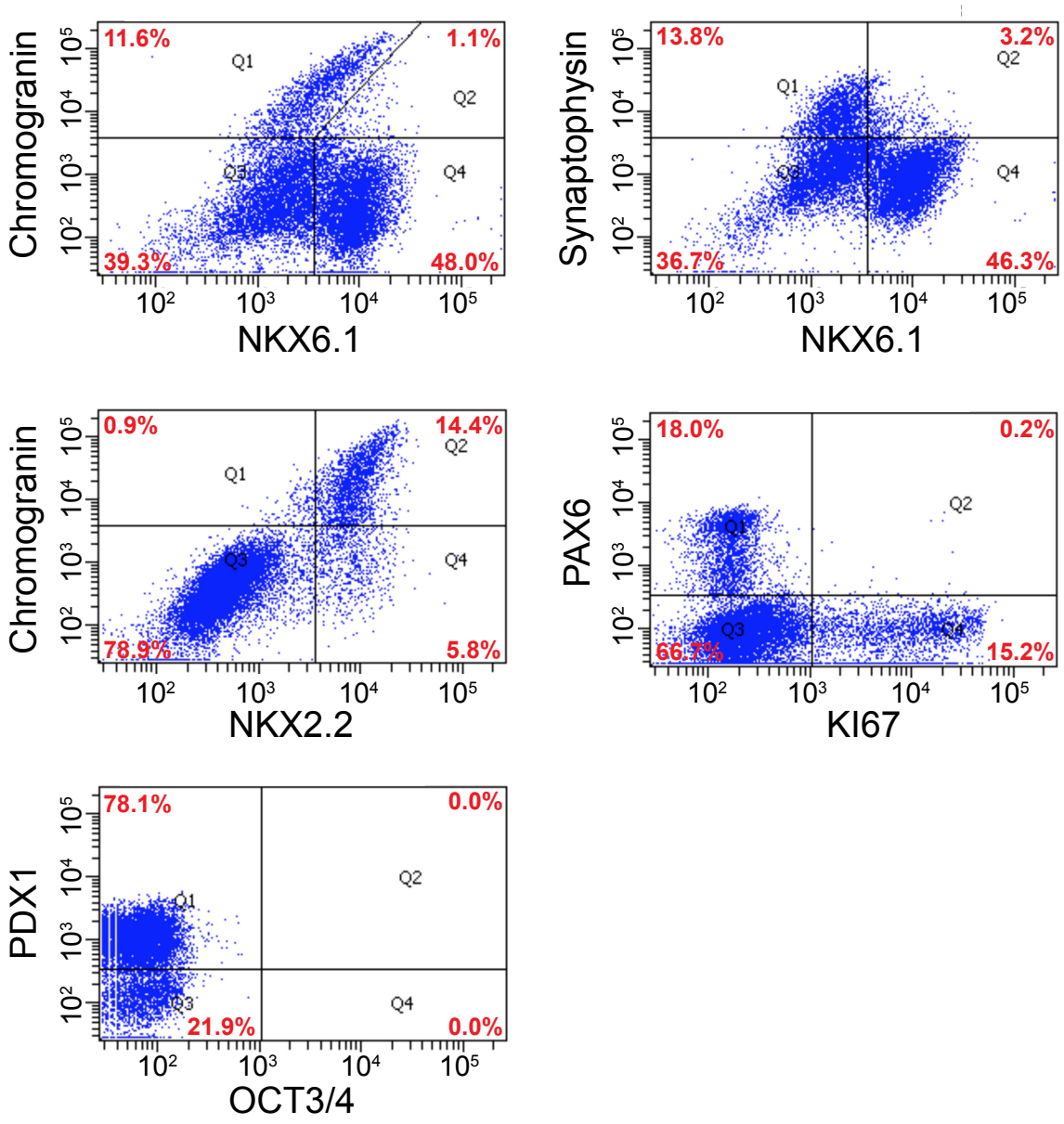

Figure S1: FACS characterization of hESC-derived pancreatic progenitor cells (related to all main figures). After the 14 day *in vitro* differentiation, the population of hESC-derived cells was characterized by flow cytometry prior to transplantation into SCID-beige mice or nude rats.

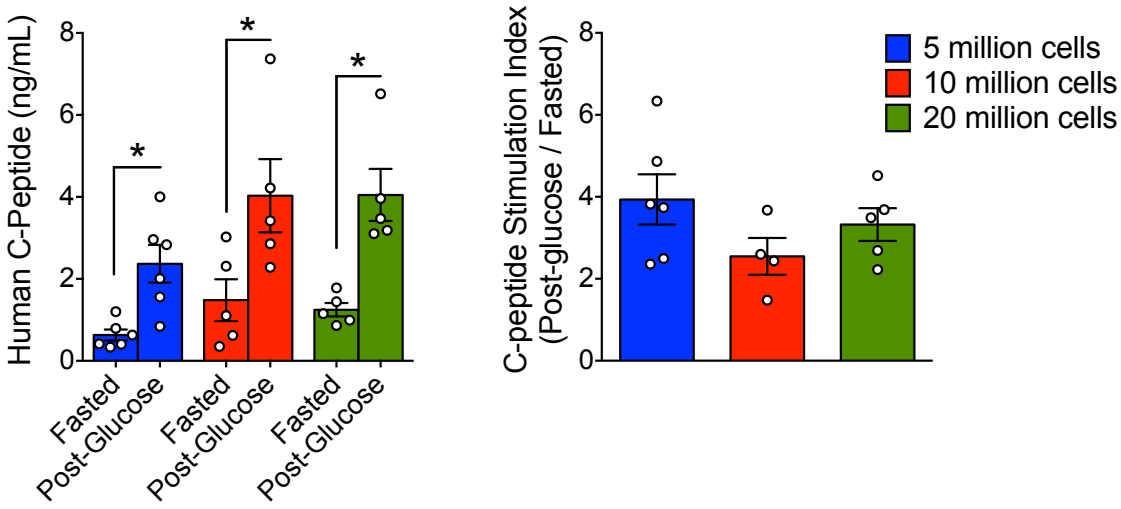

Figure S2: Dose of pancreatic progenitor cells does not affect the maturation of hESC-derived insulin-secreting cells *in vivo* (relevant to all main figures). Human C-peptide levels after an overnight fast and 60 minutes following an i.p. glucose injection (2 g/kg) at 28 weeks post-transplant of either 5, 10, or 20 million hESC-derived pancreatic progenitor cells. The C-peptide stimulation index was calculated as the human C-peptide levels post-glucose relative to fasting levels. * $p<0.05$, paired t-test (fasted vs post-glucose). Data are presented as mean ± SEM plus individual biological replicates (n=4-6 mice per group).

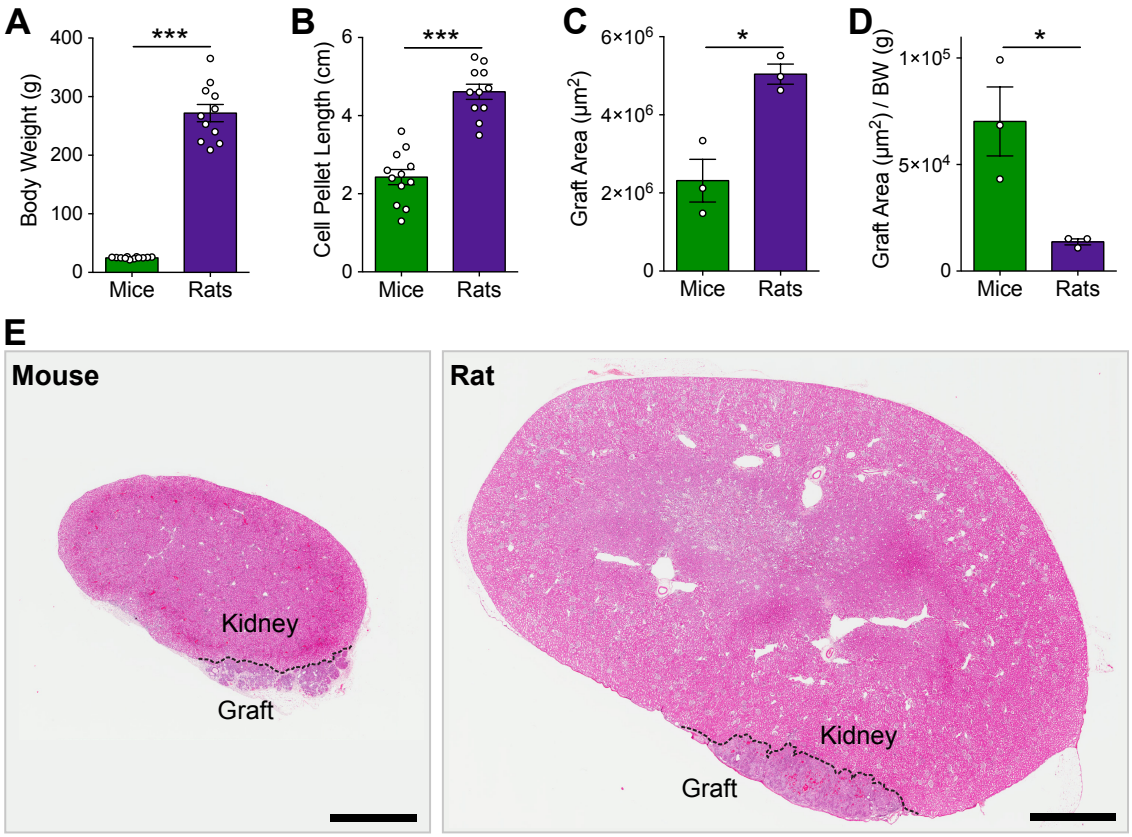

Figure S3: Graft size was disproportionate to body size in rats compared to mice (related to Figure 1). A) Body weight of SCID-beige mice and nude rats at the time of cell transplant (n=11-12 animals per group). **B)** Length of the compact cell pellet implanted into mice versus rats. **C)** Area of engrafted cells under the kidney capsule at 22 weeks post-transplant and **D)** graft area expressed relative to body weight (n=3 animals per group). **E)** Representative images of engrafted kidneys stained with H&E. Black dashed line indicates the boundary between the hESC-derived cells and kidney. Scale bars = 2 mm. *p<0.05, ***p<0.001, two-tailed t-test. Data are presented as mean ± SEM plus individual biological replicates.

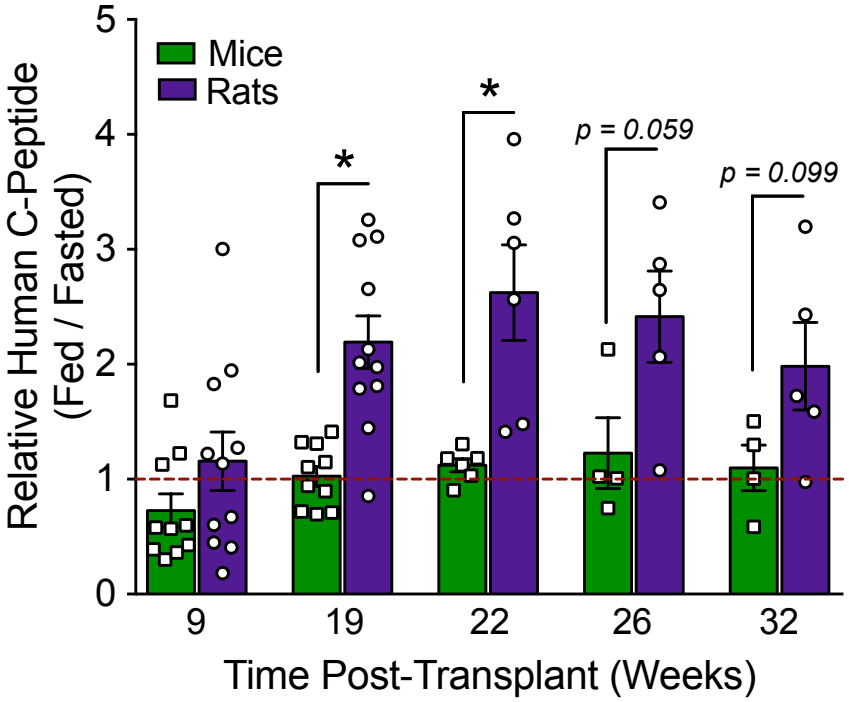

Figure S4: Human C-peptide secretion stimulation index following a meal challenge was improved in rats compared to mice (related to Figure 1A). Human C-peptide levels were measured in mice and rats after an overnight fast and 45-minutes following an oral gavage of a mixed meal (Ensure) at various time points between 9 and 32 weeks post-transplant. Data are expressed as the fed C-peptide levels relative to the fasted levels; dashed red line indicates the level at which there was no C-peptide stimulation following the meal challenge. * $p<0.05$, two-tailed t-test. All data are presented as mean ± SEM plus individual biological replicates (n=4-11 animals per group).

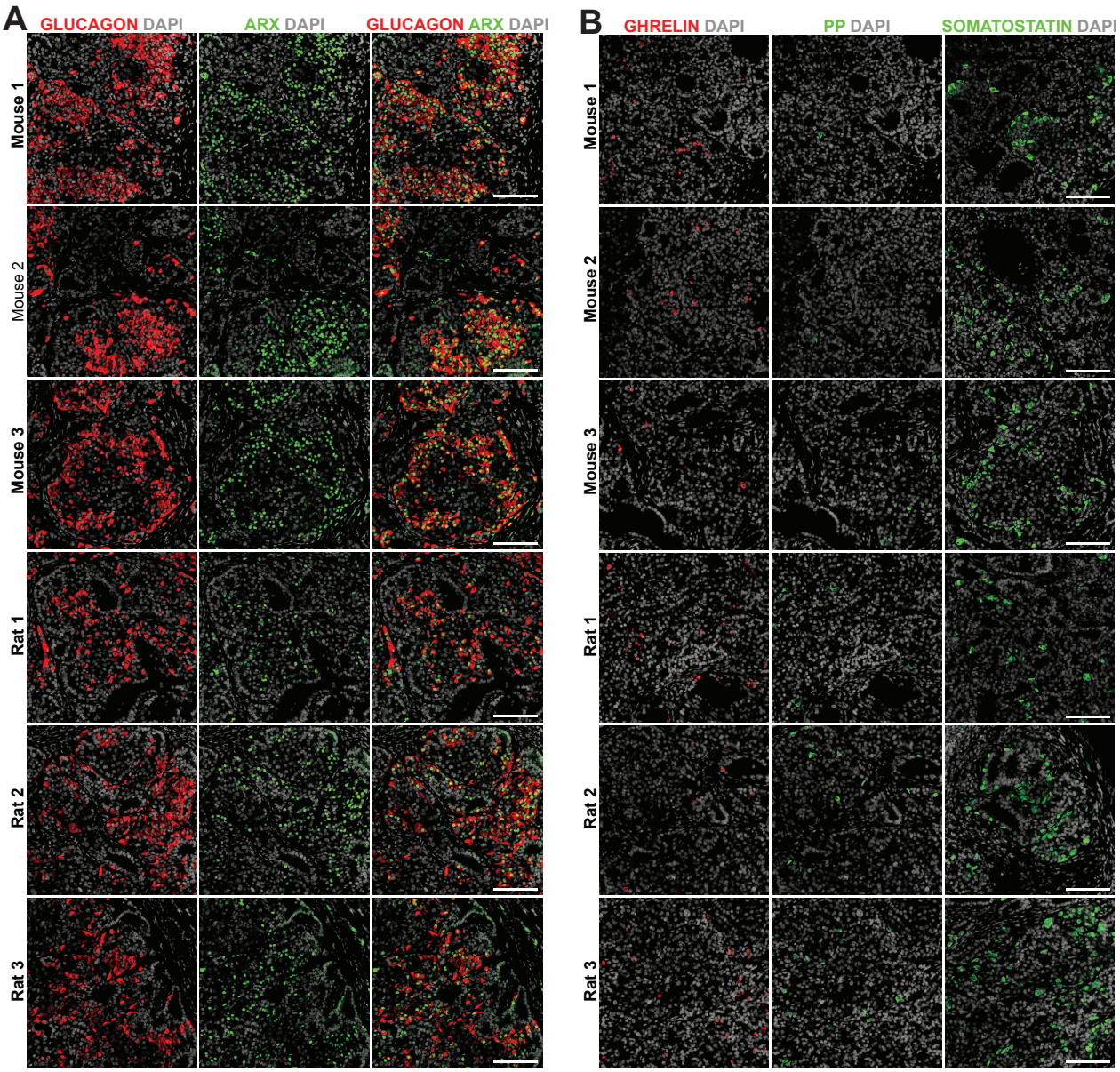

Figure S5: hESC-derived glucagon-positive cells uniformly co-expressed nuclear ARX, and all pancreatic endocrine cell types were detected in grafts from both species (related to Figures 3 and 4). Representative immunofluorescent staining of hESC-derived cells for: **A)** glucagon (red) and/or ARX (green), and **B)** ghrelin (red), pancreatic polypeptide (PP; green) or somatostatin (green). DAPI nuclear staining is shown in grey. Scale bars = 100 μm.

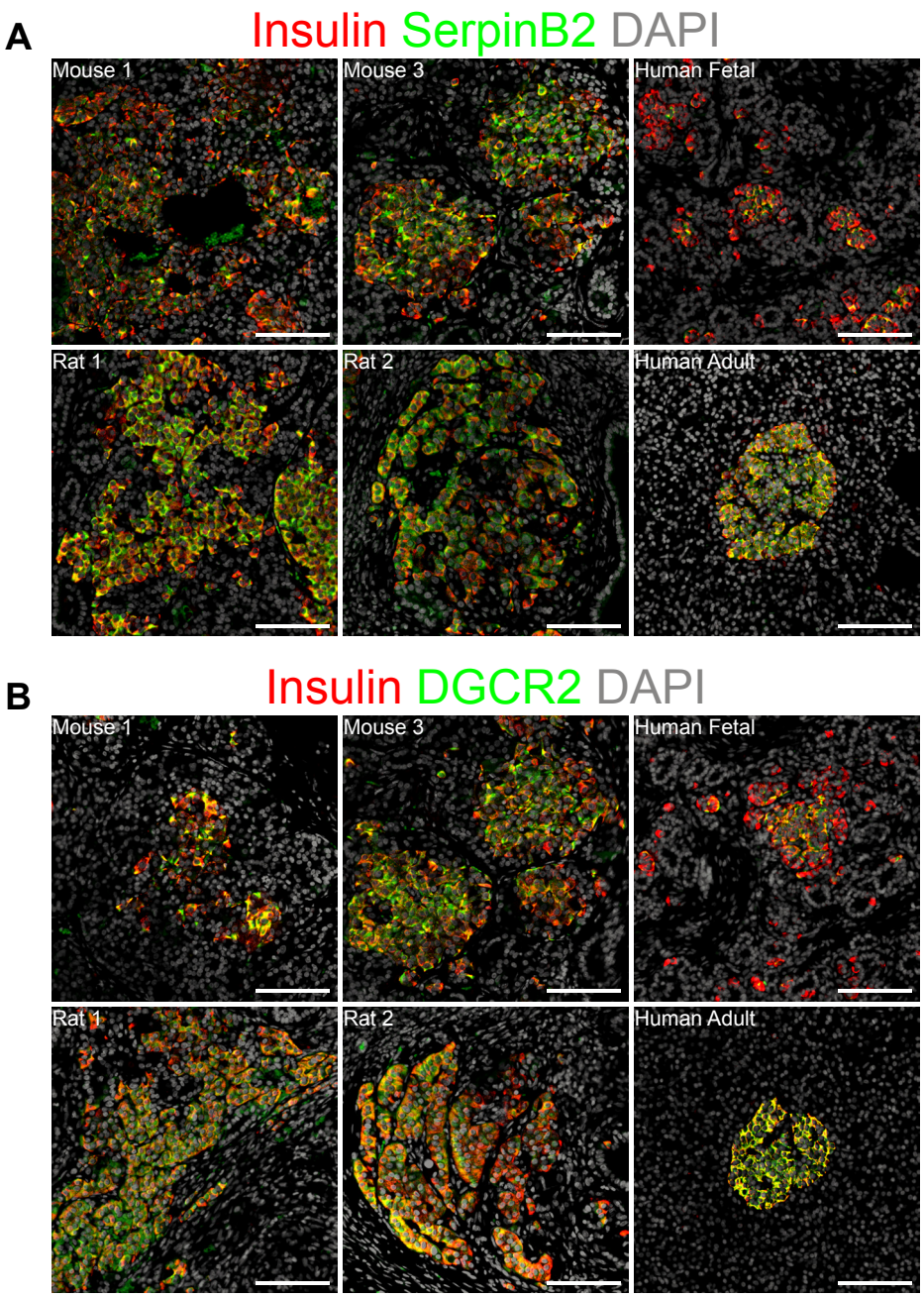

Figure S6: hESC-derived insulin-positive cells from rats more uniformly co-express SerpinB2 and DGCR2, markers of mature beta cells, compared to mice (related to Figures 4 and 5). Representative immunofluorescent staining for insulin (red) and either: **A)** SerpinB2 or **B)** DGCR2 (green) in hESC-derived grafts, human fetal pancreas tissue (gestational week 13), and adult human pancreas tissue. DAPI nuclear staining is shown in grey. Scale bars = 100 μm.

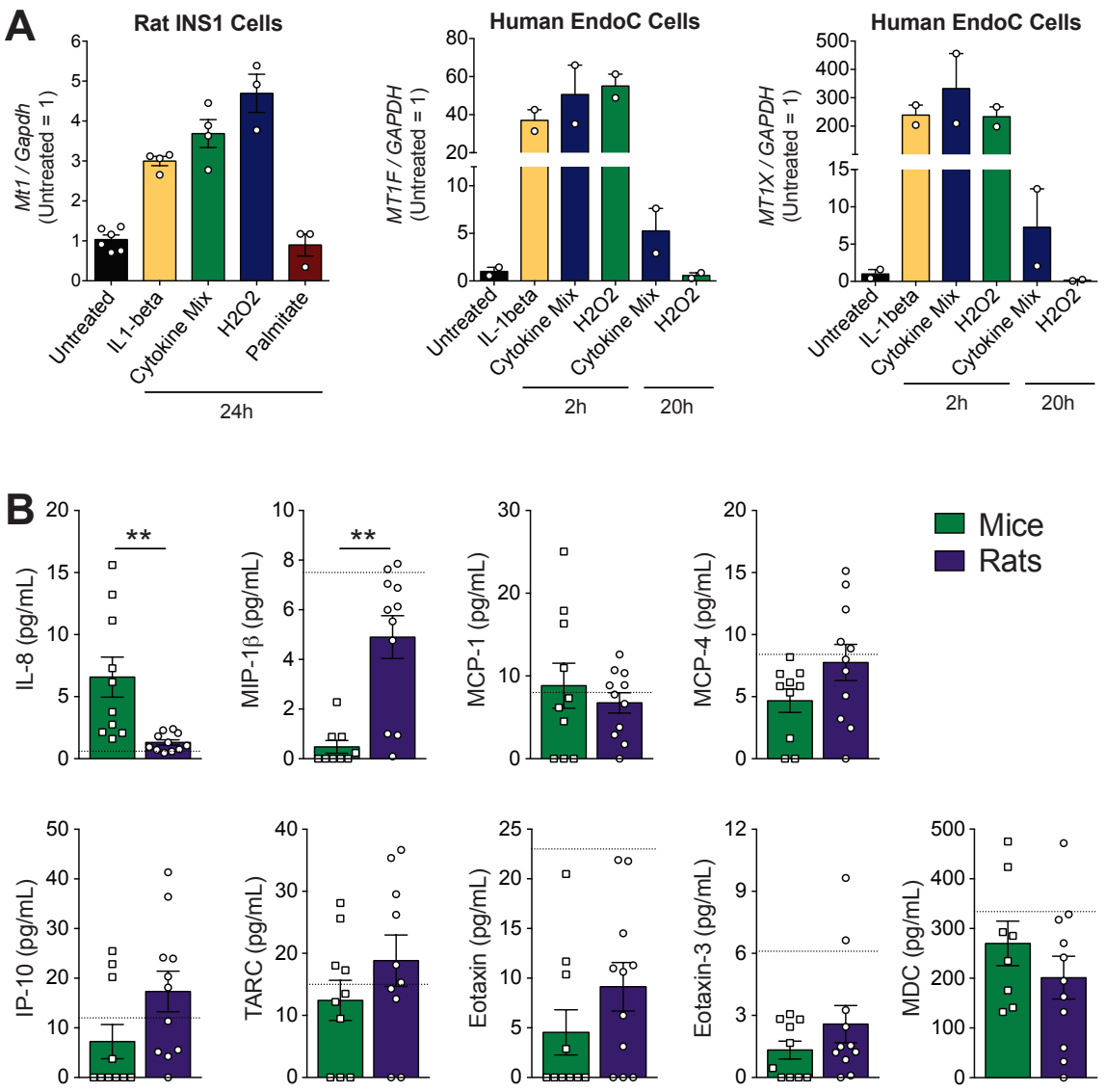

Figure S7: Induction of metallothionein 1 by cytokines and oxidative stress in beta cell lines, and human cytokine levels in transplant recipients (related to Figure 7A). A) Gene expression of metallothionein 1 (*Mt1*, *MT1F,* and *MT1X*) in a rat beta cell line (INS1; n=3-6 technical replicates per group) and human beta cell line (EndoC; n=2 technical replicates per group) following treatment with either IL1β, a cytokine mixture (IL1β, TNFα, and IFNγ), hydrogen peroxide (H_2O_2), or palmitate for 2, 20 or 24 hours. Gene expression of *Mt1/MT1F/MT1X* was expressed relative to the housekeeping gene *Gapdh/GAPDH* and normalized to untreated controls. Data are presented as mean ± SEM plus individual technical replicates. **B)** Levels of nine human cytokines in plasma from mice and rats at 22 or 33 weeks post-transplant. Dashed black line indicates the lower limit of detection on each assay. ** $p<0.01$, two-tailed t-test. Data are presented as mean ± SEM plus individual biological replicates (n=10-11 animals per group).